2003

Forced Bubble Columns

Jia Ma
Louisiana State University and Agricultural and Mechanical College, jiamawood@gmail.com

FORCED BUBBLE COLUMNS

A Thesis

Submitted to the Graduate Faculty of the
Louisiana State University and
Agricultural and Mechanical College
in partial fulfillment of the
requirement for the degree of
Master of Science in Chemical Engineering

in

The Department of Chemical Engineering

by
Jia Ma
B.S., Tianjin University, 1995
M.S., Beijing University of Chem Tech, 2000
December 2003

Acknowledgments

I would like to thank my advisor Dr. F. Carl Knopf for his original idea and endless efforts on the project. Mechanic work from Chemical Engineering shop is also highly appreciated. Without them, the buildup and operation of the units will go nowhere. Dr. Kerry M. Dooley also supported us in many ways, such as labview data collection system. The last, but not least, I would also like to give my sincere thanks for Dr. Dimitris E. Nikitopoulos for suggesting glass injectors, interpretation of phenomena inside injector and use of different membrane thickness and his work on digital photographs. His suggestions and digital camera system really played a key part in revealing the bubble breakup mechanism.

Table of Contents

List of Tables

List of Figures

Abstract

In many chemical, biochemical and pharmaceutical industrial processes, bubble breakage is very important for gas component to dissolve and react with surrounding liquid. The overall mass transfer performance can be improved greatly when the interfacial gas-liquid area is increased due to bubble breakup. In forced bubble columns operating at low forcing frequency (<30Hz) and small forcing amplitude (<3mm), bubbles undergo phenomenal breakage. Mass transfer coefficient, $k_L a$, is increased to 250%~625% of the no forcing value depending on flow regime and configuration of membrane and piston. Two different mechanisms, induced shear slug breakage in the gas feeder tube for bubbly flow and resonant frequency bubble breakage in the column fluid phase for jet flow, seem to at work.

Introduction

Bubble breakage is very important for many chemical, biochemical and pharmaceutical industrial processes. It will increase the interfacial area and favor mass transfer rate between phases. The principal goals of our experimental and theoretical work on this project are to observe and study mechanisms governing bubble breakup in the vibrating bubble column, the key operation variables and their effective range, the extent of bubble breakup and percentage of mass transfer enhancement. The potential application of such studies are gas-liquid reactors, fermentation vessels and mixing units where gas-liquid mass transfer is the rate controlling step.

Surface tension and fluid dynamics are the major physical properties influencing bubble stability. It is generally believed that bubble breakage is caused by shear stresses, generated by gas-liquid velocity differential. Gas bubbles are deformed by the shear stresses between gas and liquid after their formation in liquid. If the local shear rate is large enough, gas bubbles will experience severe distortion even result in breakup.

To improve mass transfer performance of the commonly used bubble column, a variety of configurations has been industrially adopted. Mechanically stirring bubble column is the well accepted way, which features high shear rates smashing large bubbles and greatly improves interfacial area and mass transfer. However there are several disadvantages causing attention at the same time. First, the energy consumption per unit volume is relatively high for stirring bubble column, especially at the production scale. Second, it is also difficult to model the bubble column with multiple impellers due to the non-ideal mixing effects. The third disadvantage relates to the considerable gas re-circulation in the bubble column. Recirculating of gas bubbles is unfavorable because the overall driving force for the reaction is decreased. The last disadvantage lies in the simultaneous existence of high and low shear zones even dead corners. Some bacterial cells in aerobic fermentation processes located in high shear zones of stirring bubble column may suffer death while others in low shear zones or dead corners may not develop well enough. Based on such consideration, impellers are replaced by compressed air to improve mixing and gas-liquid mass transfer under some circumstance. Though the resulting lower shear levels lead to less damage to shear sensitive organisms, the volumetric mass transfer coefficient, $k_L a$, and the corresponding volumetric production are restricted to achieve. Therefore the exploration of alternatives to improve gas-liquid mass transfer has become our interest.

According to the collaboration of Mechanical and Chemical Engineering at LSU, active forcing is able to improve spray combustion efficiency. At the resonant frequency of active forcing, both the flame temperature and OH radial temperature were much higher and more stable near the flame start than those of unforced case. Besides, Oscillatory flow generated by low frequency vibration has the potential to realize the goal of enhancing mass transfer. According to literature, under low forcing frequencies (below 100 Hz), oscillatory flow can enhance mixing, increase residence time distribution, influence bubble shape, reduce bubble size and improve gas-liquid mass transfer. So active forcing will be effective on mass transfer in the gas-liquid system.

There are several striking benefits of using low-frequency vibrations instead of mechanical agitation. First, the overall plug flow character of the gas bubbles is maintained without much energy input to re-circulate the liquid. Second, effective mixing extent and gas-liquid contacting can be achieved by controlling vibration frequency and amplitude. The third benefit is that vibrating bubble column creates self independent environment without intrusion of stirring impellers. The last but maybe the most important advantage, gas-liquid contacting is free from shear gradients caused by stirring impellers, which is absolutely required by the shear sensitive process.

Bubbly flow and jet flow are the two flow regimes that our vibrating bubble column mainly experiments on. At low gas superficial column velocities, bubbles are quite uniform in size at the same height in the column. They move up in orderly fashion with little contacting among bubbles and the liquid is mildly stirred by the bubbles. This is bubbly flow, also named homogeneous or quiescent flow. On the other hand, jet flow occurs when the gas superficial column velocity is so high that bubbles of different sizes can be found at the same height in the column. Due to the interaction among bubbles and liquid, the system is stirred up significantly, leading to increased mixing intensity.

The experimental work was done on influence of vibration frequency and amplitude on bubble size and number, gas hold-up and gas-liquid volumetric mass transfer at bubbly or jet flow in vibrating bubble column. The theoretical work was done on analyzing the bubble breakup mechanism by the high speed photos taken on whole glass nozzle, modeling the vibrating bubble column as forced and damped oscillator and applying stability prediction of T. B. Benjamin & F. Urell to the plane free surface of vibrating bubble column.

The research results show that low frequency vibration, under 30 Hz, can generate phenomenal bubble breakage observed by high speed motion analyzer. The mass transfer coefficient increase, determined by oxygen probe, are about 150% to 525%, depending on flow regime and configuration of vibrating membrane.

Induced Momentum and Resonant Frequency Bubble Breakage

Bubble column reactors (BCRs) are well known to produce effective gas-liquid contact. These reactors have few moving parts and low operational costs. Of key importance in bubble column operation is the generation of small bubbles to promote large interfacial area between gas and liquid. However, it is difficult to forecast or predict the behavior of BCRs owing to the highly chaotic nature of bubble swarms. Even the method of gas injection (single orifice, perforated plate, perforated rubber sheet, or sintered disk) has a measurable effect on performance. The process of bubble breakage and coalescence is still not well understood, and the mechanism for the onset of liquid circulation is a major unknown.

The original idea for this project grew from a collaborative effort between Mechanical and Chemical Engineering at LSU to use active forcing to improve spray combustion efficiency (Santhanam, et al., 2002). Active forcing involves the modulation or pulsing of the fuel streams and air streams to a combustor, at the acoustic resonant frequency of the combustor. The basic concept is that acoustic modulation of the primary airstream strengthens the coherent vortices of the flow field. The injection of the fuel droplets at the onset of vortex roll up provides better mixing between the droplets and the airstream leading to improved combustion efficiency. As shown in Figure 1 below, the air stream is forced using speakers and the fuel is forced by controlling the duration and timing of the fuel injector. Resonate frequency for the combustor occurred near 200 Hz for both the air and fuel streams. At the resonant frequency, both the flame temperature and OH radical concentration were much higher and more stable near the flame start (compared to the unforced case); flame temperature and OH radical concentration are indicators of combustion efficiency.

We wanted to extend the concept of active forcing to other chemical reacting systems. Forcing is known to be effective for gas reacting systems (systems that involve 2 or more gas streams) or gas and liquid droplet systems (spray combustors). Active forcing of a BCR would involve a gas / liquid dispersions.

Two years ago we constructed the BCR shown below in Figure 2. The system has a flexible rubber sheet at the base of the column. This rubber sheet seals the bottom of the column and the sheet is located between two metal plates. There is a direct coupling between the metal plates and a circular eccentric cam driven by a variable speed motor; this is analogous to the cam and piston drive in an automobile. Sine waves ranging from 0 - 100 Hz with amplitude 0 - 2.54 cm can be produced.

Several generations of design were necessary before a system allowing continuous operation was developed. It is important to note, that by changing the diameter of the metal plates holding the rubber sheet we vary column operation from a flexible piston to the equivalent of a solid piston at the column base.

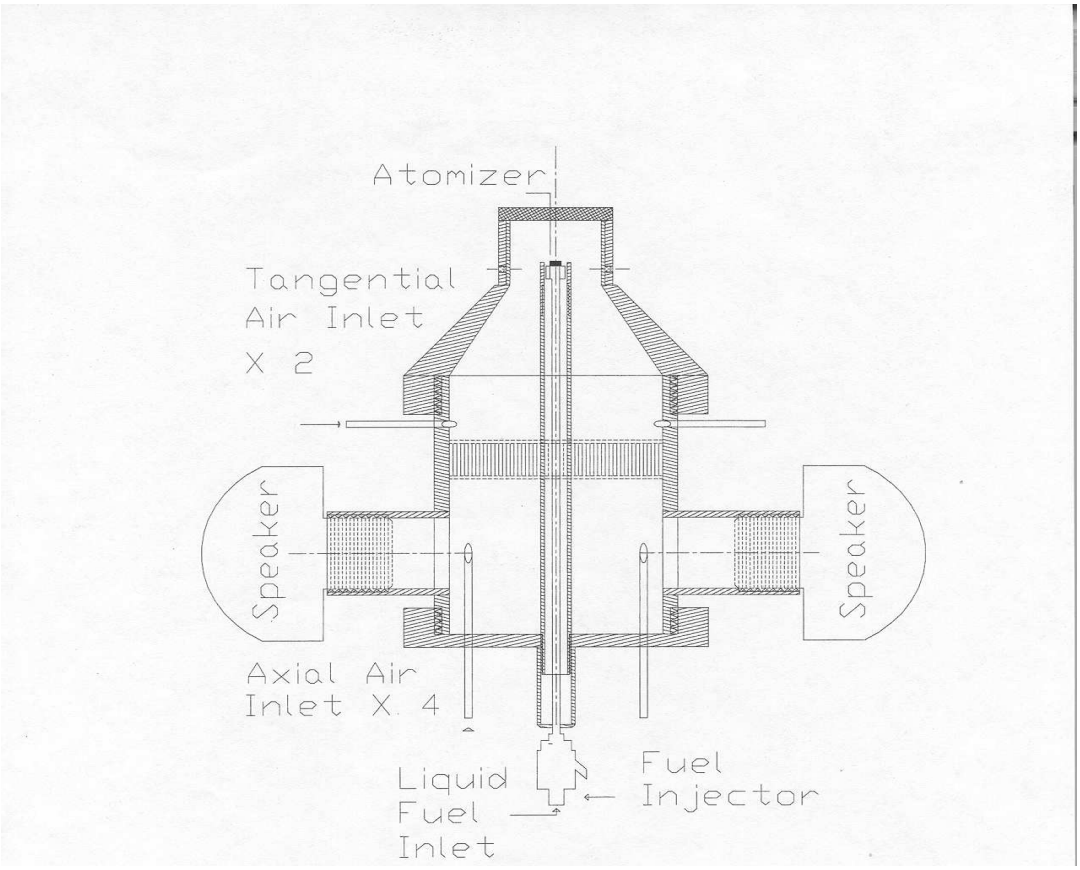

Figure 1. Forced Combustor

Initially we thought intense bubble breakage would arise at or near the column resonant frequency. In other words, at some column dependent frequency, bubbles would oscillate, become unstable followed by fragmentation. There is both experimental and theoretical evidence that instability can be created at the free surface of a liquid filled column (Benjamin and Ursell, 1954) at low frequencies. It was hoped this same instability would be created at the gas-liquid interface of the bubbles, ultimately leading to breakup.

However there are also theoretical predictions that the resonate frequency needed to break a spherical bubble is high. For example, a 3mm diameter bubble was calculated to have a natural frequency of 2200 Hz (Minnaert, 1933), which is the natural resonance of this bubble.

Using the BCR shown below we performed preliminary experiments over a range of gas flowrates, forcing frequencies and forcing amplitudes. By taking high speed photographs (1000 frames persecond) we have established that at least two different mechanisms can lead to bubble

breakup in forced oscillating columns. These two mechanisms are a.) induced shear slug breakage in the gas feeder tube and b.) resonant frequency bubble breakage in the column fluid phase. Resonant frequency bubble breakage results in the most dramatic improvement in column operation. The dominate mechanism is determined in large part by gas flowrate. For initial experiments, a single gas injector (a glass or stainless steel tee with identical i.d.) was used.

At lower gas flowrates (0~15 ml/s-injector) we have found substantial bubble breakup can occur at frequencies below 30 Hz. At these low flowrates, and with appropriate forcing amplitude and an appropriately designed injector, bubble breakup occurs in the injector itself. Here the primary cause of breakup is intense shearing of bubble slugs within the injector which fragments slugs into minute bubbles.

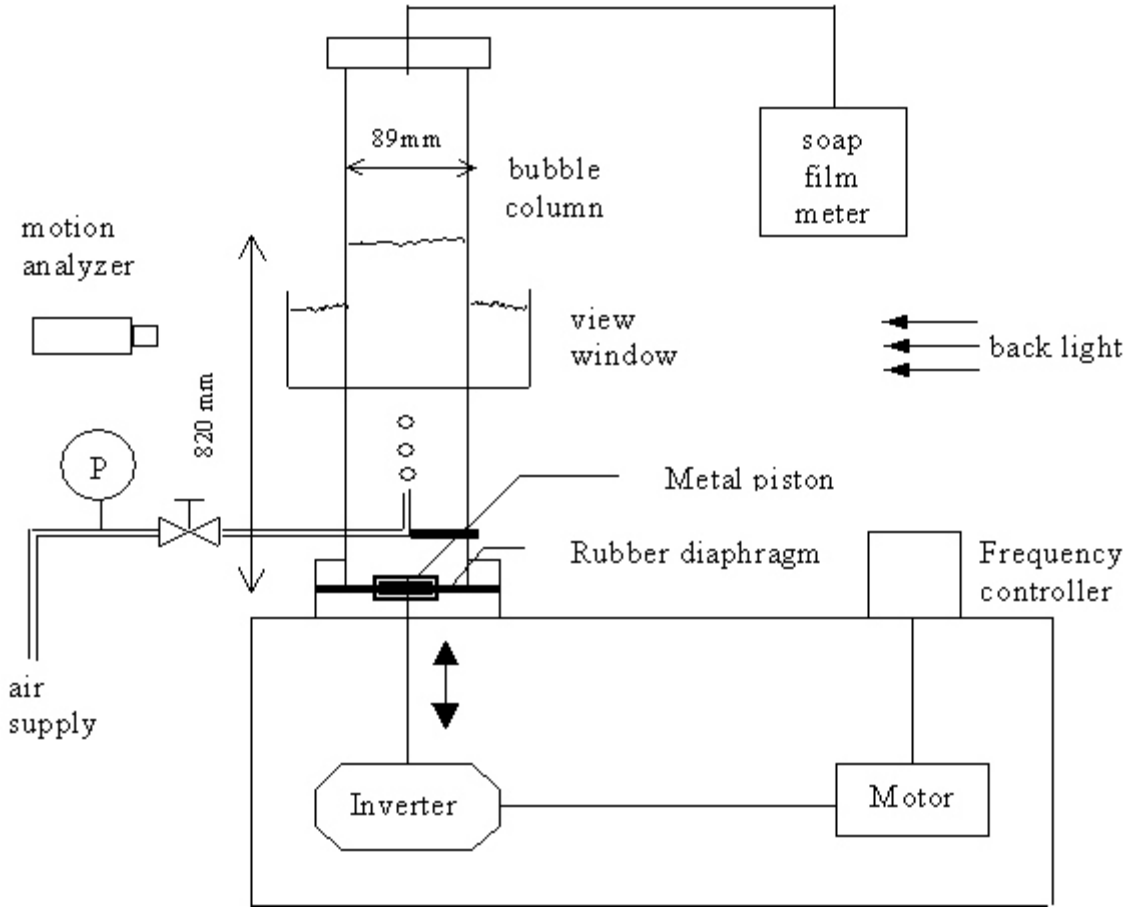

Figure 2. Illustration of vibrating bubble column reactor

At higher gas flowrates (15 to 35+ ml/s-injector, or jetting conditions) there is formation of large ill-defined bubbles. Here, column oscillation below 30 Hz, with appropriate forcing amplitude, can lead to substantial bubble breakup which we attribute to resonance effects within the tested column. This effect may extend above the 35 ml/s-injector used in the present work.

The observed induced shear bubble-slug breakage is a new finding which we quantified by careful use of a glass gas injector system and high speed photography. Resonant frequency bubble breakup in the column proper has been observed in the literature, but the forcing frequency was generally >100 Hz **not** the nominal 10Hz values we observed.

The two bubble breaking mechanisms (induced shear breakage and column resonance) are distinctly different. At lower gas flow rates, the oscillating liquid creates a suck-back during bubble formation then expulsion of water-gas slugs, in the gas feeder tube. Liquid shear on the walls of the gas feeder are observed to cause fragmentation of the gas slugs. This shearing of gas slugs causes breakage of the unstable slug flow thereby increasing the number of bubbles in the ejection cycle. At higher gas flowrates suck back in the gas feeder tube is not observed owing to higher pressure in the feeder tube, relative to the applied oscillations on the liquid in the column proper.

At higher gas flowrates there seems to be a different mechanism leading to bubble breakup. As detailed below, it is important to appreciate that the sinusoidal forcing on the liquid produced by the bottom piston introduces standing nodes on the top water-air surface. At certain frequencies and amplitudes, these waves become unstable. We have observed that operating at the instabilities on the free surface coincides with dramatic improvements in column performance. This is a clear extension of the effects predicted by the hydrodynamic analysis of Benjamin and Ursell (1954).

Throughout this project we maintain all experiments in a frequency range of 0 - 30 Hz and amplitudes were held below 3mm, which would be suitable for industrial applications.

In this paper / proposal we provide details of the experimental setup and explanations of data collected to date. Initially we separate the low bubbly flow and jet flow phenomenon. Later, we combine all data to clearly show that different mechanisms are involved. An experimental and theoretical framework is provided which will allow quantification and extension of this technology. This technology can yield substantial energy reductions and improved mass transfer (Connell, 1972) in gas / liquid contact systems including for example, fermentations, distillation and waste water treatment processes. The technology can be extended to multi- phase reaction systems, for example, certain phase transfer catalytic processes and some micro-reactor systems where gas injection is needed, but desired bubble size is difficult to obtain.

Experimental and Procedures

Equipment

The experimental equipment consists of a bubble column with a single injector. The bubble column is constructed from Plexiglas and is sealed with a natural gum rubber sheet. The equipment is shown in Figure 2. For all experiments, air was introduced into the system through a single injector with an i.d. of 0.75mm. This injector was either stainless steel or glass. Care was taken to insure no burrs were present at the injector tip; a stereo microscope was used for this purpose. The gas flow was controlled by use of a pressure regulator and a metering valve. Gas flow rates were measured using a soap film meter. The water used in the column was carefully distilled and deionized.

The natural gum rubber sheet at the base of the column is clamped between 2 stainless steel disks. These disks are directly coupled to an eccentric cam which is driven by a five horsepower variable speed motor. The motor speed is controlled by an Omron Sysdrive 3G 3JV compact inverter controller. The eccentric cam produces a true sinusoidal oscillation in the disks / rubber sheet at the base of the column (Rodriguez, et al., 2003). The system is initially configured for operation from 0 - 30 Hz and amplitudes from 0 to 2.54 cm. By changing the pulley system, operation to 100Hz is possible.

As will be detailed below, there are both theoretical and practical reasons for exploring both a flexible membrane piston and solid piston forcing at the column base.

Flexible Piston

Here the natural gum rubber sheet at the base of the column is clamped between 2 stainless steel disks each 2.73 cm in diameter. The column diameter is 8.9 cm, which effectively allows pulsation of 56.3 cm^2 of rubber at the column base. As we learned, the rubber membrane acting as a piston sustained its own dynamics. At high frequency, the movement of the membrane was not in phase with the movement of the steel disks.

Solid Piston

Here the natural gum rubber sheet at the base of the column is clamped between 2 stainless steel disks each 8.26 cm in diameter. This allows pulsation of a maximum of 2.74 cm^2 of rubber at the column base, which will behave more like a solid piston.

The experimental set-up allows control of the gas flow rate, amplitude, and frequency of vibration. At each experimental condition measurements of gas hold up, $\in$, and mass transfer coefficient, k_La, were undertaken. Under certain reproducible conditions, bubbles were also counted and recorded.

Voidage (Gas Hold-Up) Measurements

The gas hold up was determined by the manometric method (Burns, L.F. 1995). As indicated in Figure 2, two taps are used, one 11cm from the rubber sheet and the other 77cm above the rubber sheet. The manometer fluid is Meriam Red 295 with a specific gravity of 2.95. A pressure balance on each leg of the manometer allows voidage to be determined using,

$$\varepsilon = \left(\frac{\rho_{Mer\,red} - \rho_{water}}{\rho_{water}} \right) \frac{\Delta h}{H} \qquad (1)$$

The height differential in Meriam Red 295 was determined using a cathotometer which provided an accuracy of plus or minus 0.01mm.

Amplitude Measurements

Flexible-Piston

A key variable is the amplitude of liquid oscillation above the piston. The flexible rubber sheet acting as a piston in the column base was clamped between 2 stainless steel disks (27.3mm diameter) which were vibrated by a cam system. The metal disks are much smaller than the column diameter. The cam system produces a fixed amplitude sinusoidal motion of the metal disks. However this amplitude does not necessarily translate to a fixed amplitude for water displacement in the column.

For example, we fixed the amplitude of the metal disks at 1.36mm and used a 3.18mm (1/8") thick natural gum rubber sheet acting as the piston. Basically the rubber sheet stretches to accommodate this amplitude. By slowly turning the cam by hand and using the cathotometer to directly measure water column height change, A_0 (water amplitude as the frequency approaches 0) was determined as 0.74 mm. To determine amplitudes at various frequencies, a Styrofoam disk was placed on top of the water and filmed as a function of frequency using a high speed (1000 frame/s) digital camera (a Kodak Ektapro Integer Model 1000HRC). These results are summarized in Table 1 and plotted in Figure 3.

To confirm these results, a very slow flowrate (0.05 ml/s) of bubbles was introduced into the column and the bubbles were filmed as a function of frequency using digital camera. Bubble relative position was recorded as a function of time at fixed frequency. This allowed the bubble amplitude to be determined as shown in Table 2. Figure 3 shows the average bubble amplitude as compared to the free surface Styrofoam disk measurements discussed above. There is general agreement between the results - the large bubble amplitude at 20 Hz is being examined. A single bubble may represent the most ideal means of determining the true fluid amplitude owing to the small bubble inertia. However, the bubble must be very small, as history and virtual mass forces, as well as deformation of the bubble, may play a role in biasing results.

An inertia-visco-elastic model of the system, which allows prediction of observed amplitudes, is detailed below. To simplify reporting our data, the cam amplitude setting will be used. When appropriate for discussion, the actual fluid amplitude will be used.

Table 1: Water Amplitude versus frequency determined from Styrofoam Disk - cam amp 1.36 mm and 3.18 mm thick flexible piston

Cam F/(Hz)	Water A/(mm)
0	0.74
5	0.71
10	0.65
15	1.3
17.5	2.46
20	1.69
22.5	1.04
30	0.32

Table 2: Amplitude determined from oscillations in rising bubbles

CamF(Hz)	Bubble A/(mm)
10	0.97
17.5	2.79
20	3.77
25	1.58
30	1.07

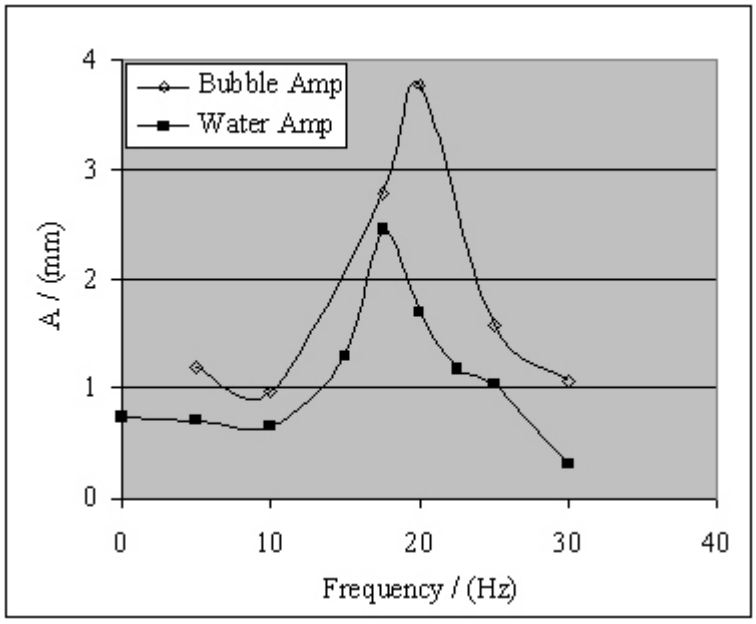

Figure 3. Amplitude vs. Frequency
(Cam amplitude = 1.36 mm, membrane 3.18 mm)

Solid-Piston

Here, the flexible rubber sheet at the column base was clamped between 2 stainless steel disks (8.26 cm diameter) which were vibrated by a cam system. The metal disks are sized close to the column diameter. The column water amplitude is simply taken as the amplitude of the metal disks.

Mass Transfer Coefficient Measurements

A key aspect of the forcing technology is to improve mass transfer. The generation of large bubble numbers, and consequently large surface area, using low energy input may allow agitator replacement with considerable savings. To investigate improvements in mass transfer, we measured the mass transfer coefficient as a function of frequency at several air flow rates and amplitudes.

For mass transfer experiments, a dissolved oxygen probe from Cole Palmer (Model 300mm) and signal conditioner (Model 01971-00) is placed in the bubble column, approximately 0.32 m above the injector. Gas bubbles do not directly impact the electrode. The column was initially purged of oxygen using nitrogen. After the dissolved oxygen content reached nearly 0 volume %, air flow was started.

The volumetric mass transfer coefficient was determined by measuring dissolved oxygen uptake in the bubble column as a function of time. Following Rice and Do (1995), the incremental rate expression for oxygen transfer (moles / time) into the liquid phase of a bubble column is given as the product of the volumetric mass transfer coefficient, multiplied by the linear composition driving force, and this times the incremental volume of the column,

$$\Delta R = k_L a\left(C^* - C\right) A\Delta z \qquad (2)$$

Here, C* and C represent the gas solubility and measured dissolved oxygen concentration (moles of solute/ cc liquid), respectively. A solute balance on the liquid phase simply states the rate of accumulation equals the rate of transfer

$$A\Delta z\,(1-\varepsilon)\frac{dC}{dt} = k_L a\left(C^* - C\right) A\Delta z \qquad (3)$$

where ϵ is the fraction void or gas volume in the column and (1- ϵ) is the fractional liquid volume (cc liquid/ cc total volume). Simplifying,

$$(1-\varepsilon)\frac{dC}{dt} = k_L a\left(C^* - C\right) \qquad (4)$$

Integration of equation (3) yields,

$$C(t) = C^* - (C^* - C_0)\exp\left(-\frac{k_L a}{(1-\varepsilon)}t\right) \quad (5)$$

where C_0 (C at t = 0) is the initial oxygen concentration (C_0 = 0 for our experiments). Rearranging yields the dimensionless dissolved oxygen concentration as a function of time and mass transfer coefficient,

$$\frac{C(t)}{C^*} = 1 - \exp\left(-\frac{k_L a}{(1-\varepsilon)}t\right) \quad (6)$$

The only unknown here is $k_L a$ (since $\in$ is measured separately), which is determined by minimizing the sum of the square of the difference between measured and predicted normalized concentration measurements. The standard regression solver in Excel was used. Concentration measurements were collected every 0.33 seconds and then every 10 data points were averaged and stored.

Results and Discussion

In the following section, data and a model are compared for water pulsation using the Flexible Piston. In order to study dynamics, three different thickness of natural rubber were used for the Flexible Piston. Following this, the new finding of Induced Shear Bubble Breakage at low gas flowrates is detailed. At higher flowrates, column resonance is observed. Column resonance provides the most dramatic results, in terms of transport properties. Resonance is explained using a model based on stability analysis of the Matheau equations as determined by Benjamin and Ursell (1954).

Amplitude- Flexible Piston

Water amplitude is a key variable. Summarized in Tables 3 and 4 are measured water amplitudes as a function of frequency for two different fixed cam settings of 0.51 mm (Table 3) and 1.36 mm (Table 4) and three different thickness of natural rubber used as the Flexible Piston. Amplitude was determined using the Styrofoam disk technique described in the previous section, Amplitude Measurements - Flexible Piston. The results in Table 3 and Table 4 show an amplitude maximum in frequency (highlighted in bold), which is a function of membrane thickness.

Table 3: Water amplitudes with cam amp 0.51 mm and 3 thicknesses of Flexible Pistons

Cam Frequency / (Hz)	water A/ (mm) 1.59 mm (1/16") mem	water A/ (mm) 3.18 mm (1/8") mem	water A/ (mm) 6.35 mm (1/4") mem
0	0.303	0.303	0.303
10	0.38	0.23	0.38
15	0.92	0.52	0.31
17.5	**1.15**	0.84	0.46
20	0.61	**1.56**	0.61
22.5	0.38	0.91	0.92
25	0.31	0.39	**1.37**
30	0.31	0.13	0.46

Table 4: Water amplitudes with cam amp 1.36 mm and 3 thicknesses of Flexible Pistons

Cam Frequency / (Hz)	water A/ (mm) 1.59 mm (1/16") mem	water A/ (mm) 3.18 mm (1/8") mem	water A/ (mm) 6.35 mm (1/4") mem
0	0.74	0.74	0.74
5	0.39	0.71	0.39
10	0.52	0.65	0.78
15	**1.69**	1.3	0.84
17.5	1.66	**2.46**	1.23
20	0.97	1.69	1.69
22.5	0.78	1.17	**1.94**
25	0.71	1.04	1.81
30	0.39	0.32	1.1

As a first approximation, the membrane water cam system can be modeled as a second order underdamped process with inertia visco-elastic behavior (IVE). Here the analogy is being made between the oscillating water column and the classic problem of the periodic forced oscillation of a body on a spring and damper. The second order differential equation for the system shown in Figure 4 is,

$$m\frac{d^2x}{dt^2} + c\frac{dx}{dt} + kx = F_o(\cos\omega t) \qquad (7)$$

Where m is the mass of the moving body (water), c the damping constant, k the spring or rubber membrane modulus, F_0 is the piston forcing function (imposed acceleration or $F_0 = A_0\,(m)(\omega)^2$), ω the frequency (radians), and x is the observed displacement.

The maximum x, or the amplitude of motion, A, was determined after transients have died out (frequency response):

$$A(\omega) = \frac{F_0}{\sqrt{m^2(\omega_0^2 - \omega^2)^2 + \omega^2 c^2}} \qquad (8)$$

Here ω_0 is the system natural frequency defined as $\sqrt{k/m}$. The value of k can be determined by measuring the displacement of the rubber membrane under increasing mass (here the mass used should be the same diameter as the metal piston). However, a simple approach is to assume the natural frequency, ω_0, of the system develops the maximum amplitude for any given thickness rubber and cam setting (for example, from Table 4, take $\omega_0/(2\pi)$ = 17.5 hz for 1/8 inch rubber membrane and 1.36 mm cam setting).

This assumptions allows direct calculation of c, the damping constant. Also note in Tables 3 and 4 that the maximum amplitude (in bold) increases with increasing thickness; k would be expected to increase with thickness. Figures 5a- f show equation (8) (with c determined at the maximum amplitude) versus the experimental data in tables 3 and 4.

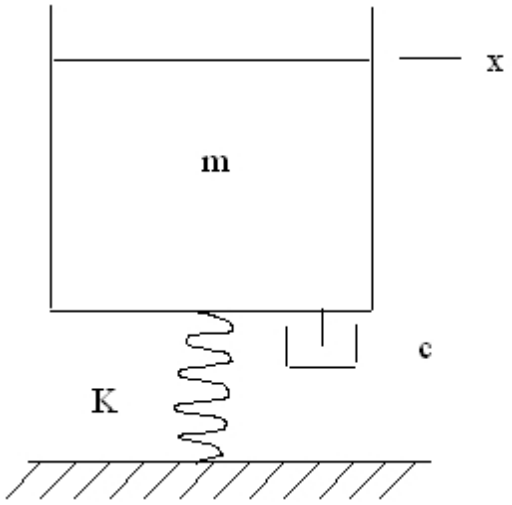

Figure 4. Conceptual mass on a spring
analogy of the water column

It is clear that resonance depends on the fixed forcing amplitude which does indicate that a 2nd order linear system model may not be best for the system. The more detailed and complicated modeling work is in progress.

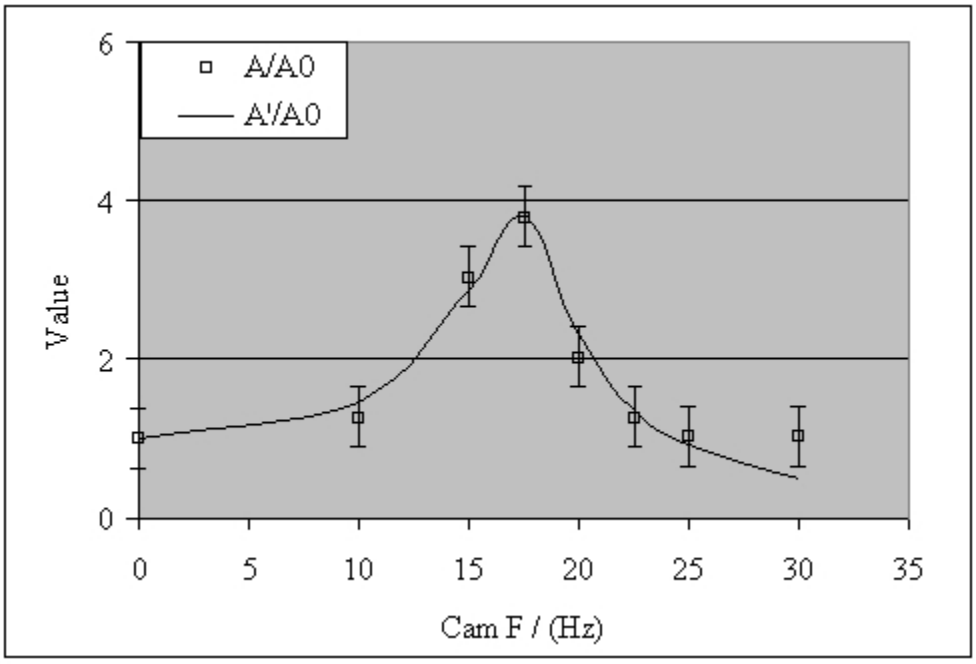

Figure 5a. Comparison of normalized water A and model A'
Membrane 1.59 mm, cam amp 0.51 mm and C = 148.7 kg/s

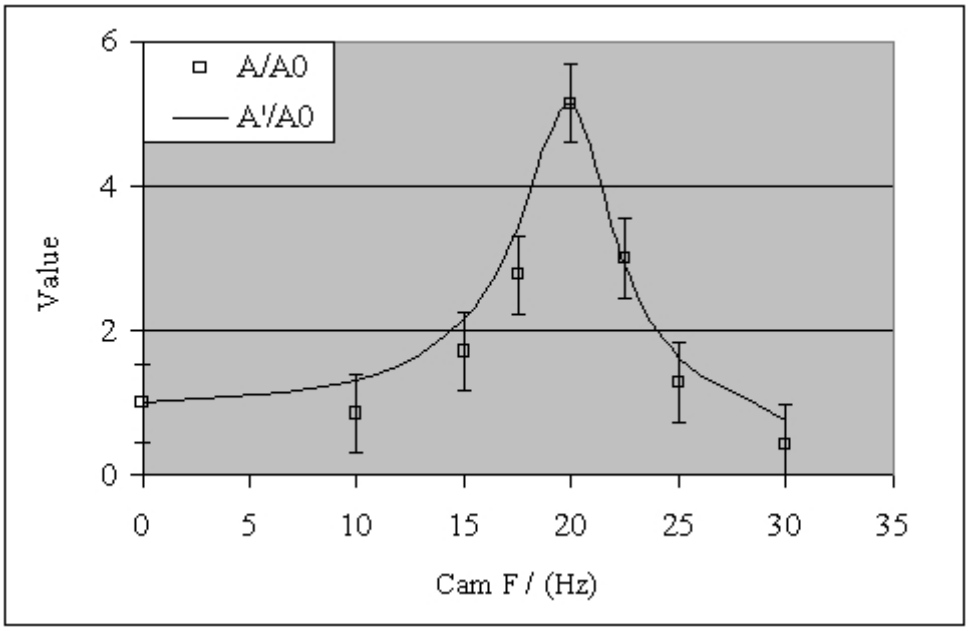

Figure 5b. Comparison of normalized water A and model A'
Membrane 3.18 mm, cam amp 0.51 mm and C = 125.44 kg/s

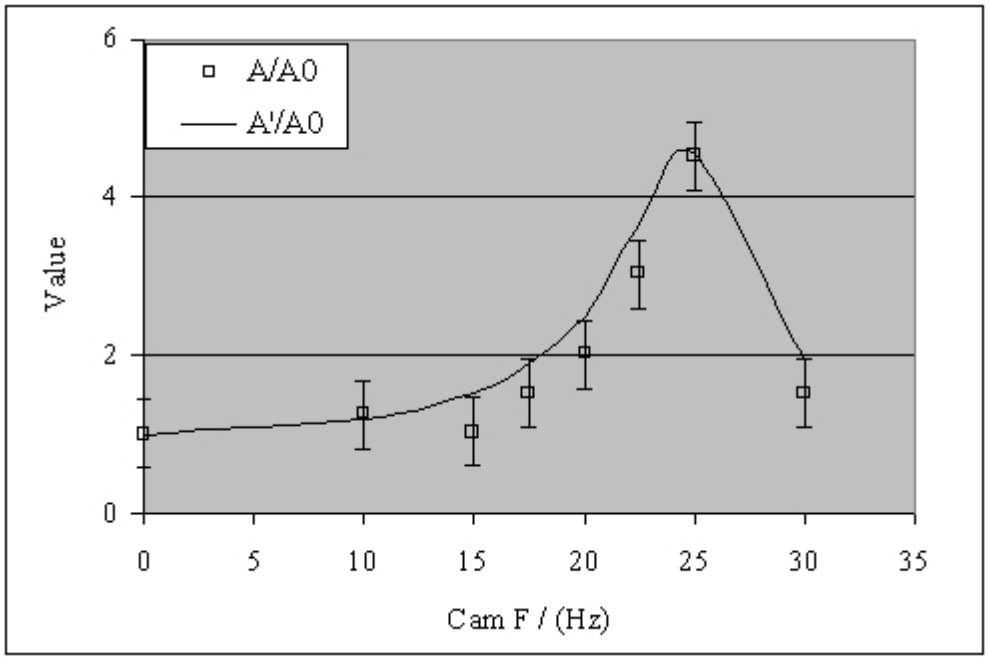

Figure 5c. Comparison of normalized water A and model A'
Membrane 6.35 mm, cam amp 0.51 mm and C = 178.65 kg/s

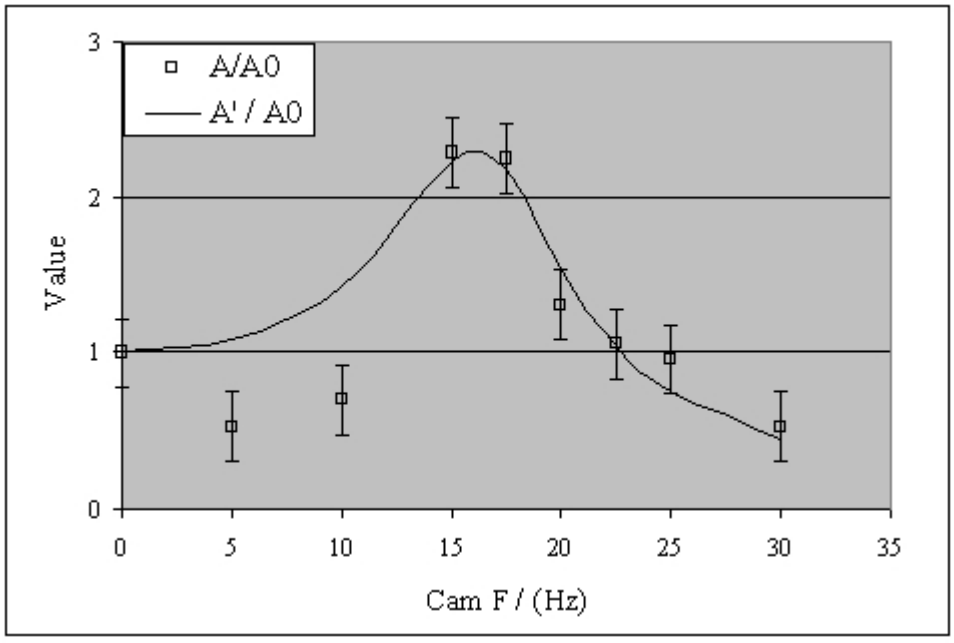

Figure 5d. Comparison of normalized water A and model A'
Membrane 1.59 mm, cam amp 1.36 mm and C = 242.96 kg/s

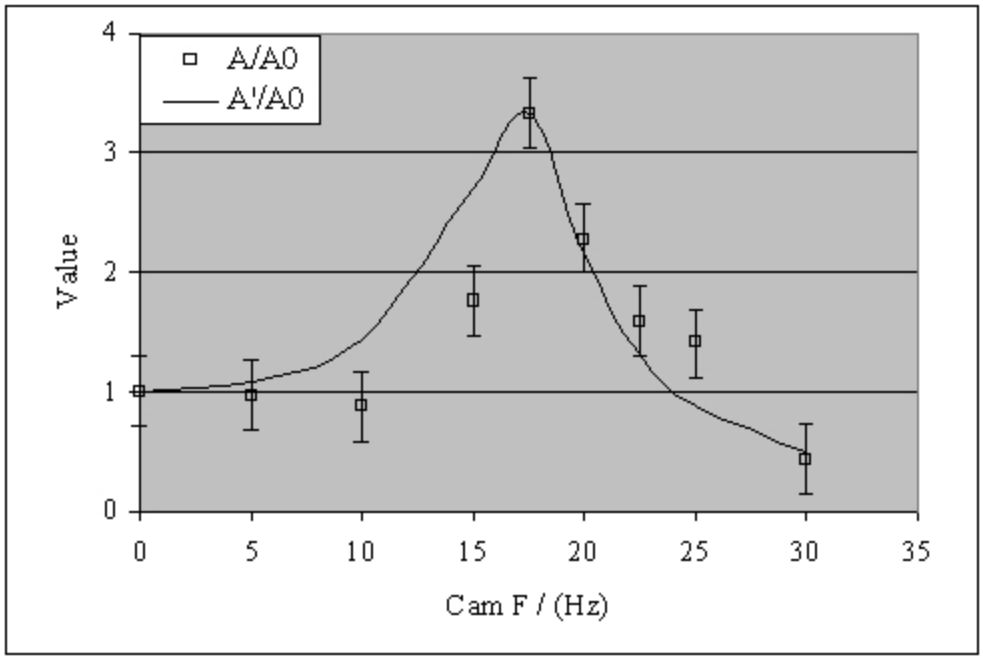

Figure 5e. Comparison of normalized water A and model A'
Membrane 3.18 mm, cam amp 1.36 mm and C = 170.25 kg/s

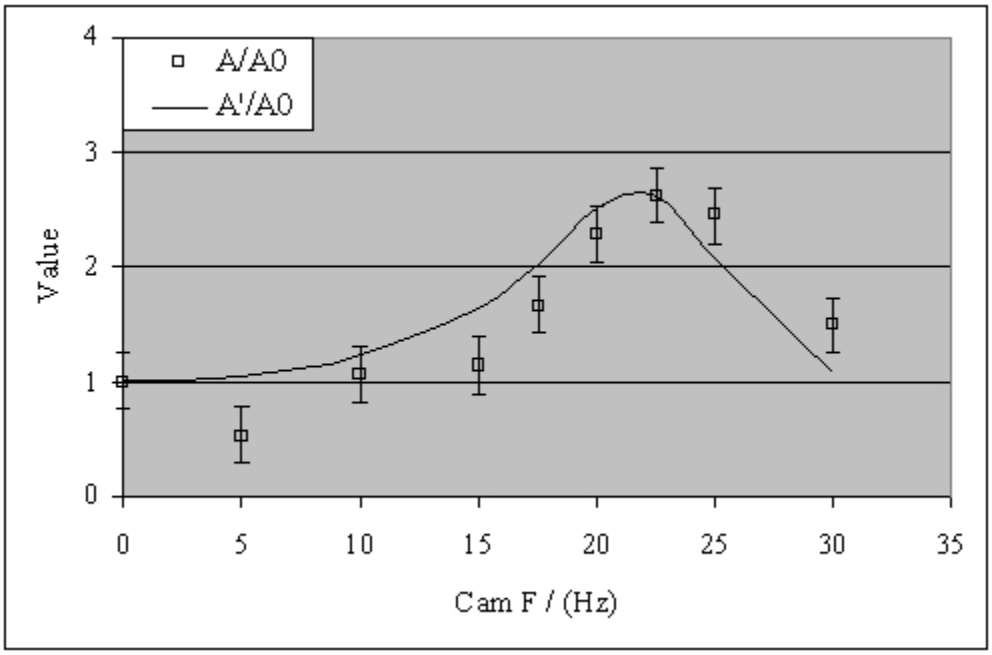

Figure 5f. Comparison of normalized water A and model A'
Membrane 6.35 mm, cam amp 1.36 mm and C = 277.38 kg/s

It is important to appreciate that without the Styrofoam float on the top water surface (used to determine the amplitudes shown above), the pulsations from the piston would normally produce standing nodes on the free surface. For example, at a cam setting of 1.36mm and using a 3.18 mm (1/8") membrane, the table below summarizes the activity of the free surface. The free surface nodes may show stable oscillations (5 - 12.5 Hz), or they may interact to produce a quiet surface (as we observed at 30 Hz), or they may interact to produce an unstable surface with sloshing as we visually observed from 15 - 22.5 Hz We suspect these surface disturbances arise from fluid mechanical instabilities. This is explored in greater detail in light of the inviscid theory of Benjamin and Ursell (1954) discussed in a later section.

Table 5: Free surface condition (with no Styrofoam on free surface), flexible piston, cam amp 1.36mm, 3.18 mm rubber membrane

F (Hz)	Free surface condition
0	Stable
5	Stable, near plug flow up and down, no droplets
7.5	Stable, no droplets, center node up and down, rings distributed
10	Stable, no droplets, 1 central node followed by 6 symmetric peaks near wall in turn
12.5	Stable, no droplets, 4 symmetric nodes around center
15	Unstable interface started, droplets formed, tens of irregular nodes, discontinuous thin water column
17.5	Unstable, no clear nodes, periodic sloshing against wall
20	Unstable but less violent, still periodic sloshing, no clear nodes, can see discontinuous water column
22.5	Unstable interface becomes flat, dozens of nodes and discontinuous water column and random droplets
25	Stable, about 20 small nodes, a few droplets formed randomly
27.5	Stable, about 30 nodes, a few random droplets and very flat
30	Very stable and flat interface, about 50 tiny nodes, few droplets

Amplitude- Solid Piston

The column water amplitude is fixed by the amplitude of the metal disks; a fixed amplitude at any frequency can be obtained.

Practical Considerations - Flexible Piston vs. Solid Piston

Based on the well known behavior of underdamped second order systems, we expected the flexible piston would show large amplitude enhancements at some forcing frequency. These forcing frequencies and amplitudes are highlighted in bold in Tables 3 and 4. The forcing frequency, with large amplitude enhancement, can be considered the practical resonance of the system. Such resonance is known to destabilize bridges, buildings, and mechanical devices. We suspected there may also be resonant enhancements in voidage and transport properties in the bubble column.

We surmised that the solid piston, when set to the same observed amplitude and frequency as the flexible piston, would produce identical results. The experimental advantage of the solid piston is that amplitude is held constant at all frequencies.

There are also industrial consideration when using a flexible piston relative to a solid piston. For industrial applications, forcing may be easier to implement using the flexible piston; it is often difficult to seal a solid piston.

Induced Shear Bubble Breakup

Induced shear bubble breakage as a mechanism is a new discovery and may explain data from other recent research (Krishna and Ellenberger, 2003). Induced Shear bubble breakup was investigated using the 3.18mm flexible piston. When using lower gas flowrates (0.18 ml/s-single injector) we observed large numbers of bubbles when very mild forcing was used (10 - 30 Hz), with a 3.18mm (1/8") thick natural gum rubber sheet, and at constant cam amplitude settings of 1.36mm and 0.51 mm (see Tables 3 and 4 for actual amplitudes). The observed pattern could be described as ideal bubbly flow. This result was entirely unexpected and not previously reported in the literature. The two photographs (Figures 6a and b) and Figure 7 below, show the rapid increase in number of bubbles as the frequency is increased.

At an air flowrate of 0.18 ml/s our single injector in the unforced BCR produced 10 bubbles/s. As shown in Figure 7, when forced at 17.5 Hz the number of bubbles increased to > 500/s. Similar results were observed at other flowrates; for example at a very low flowrate of 0.05 ml/s over 200 bubbles/s were produced at 17.5 Hz. This increase in bubble number and consequently bubble area can be used to promote mass transfer (as detailed below), generate small bubbles in micro- and nano- scale reactor systems, and improve reaction rates, for example in fermentations and phase transfer reactions. The number of bubbles/s was determined by two methods, both using a high speed Kodak camera at 1000 frames/s (Kodak Ektapro Integer Model 1000HRC).

As shown in the following section, we took pictures of bubbles leaving the injection nozzle, which allows direct bubble counting. In addition, cross sections of the column were recorded at varying distances above the injector. In this latter method, bubbles were grouped into size categories (10 diameter categories). Then the known volumetric flowrate is divided by the average bubble volume to determine the number of bubbles; this method is more approximate when compared with counting bubbles directly from the nozzle.

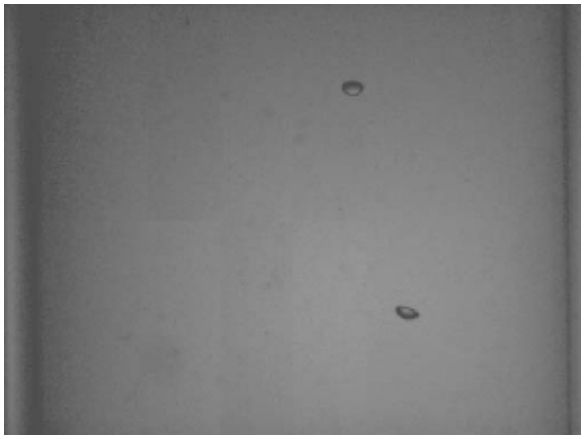

Figure 6a.
Frequency 0 Hz
membrane 3.18 mm (1/8") thick
V = 0.18 ml/s

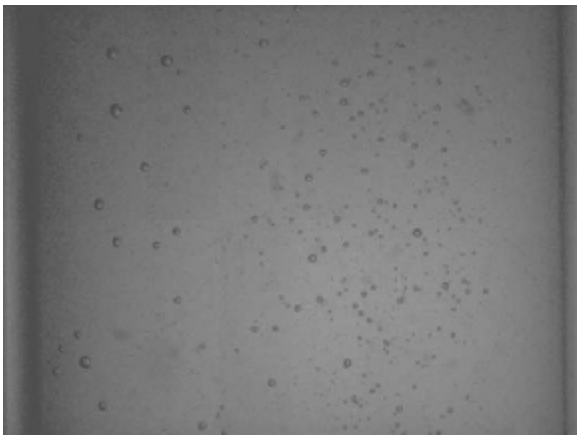

Figure 6b.
Frequency 17.5 Hz
Cam amplitude 1.36 mm
membrane 3.18 mm (1/8") thick
V = 0.18 ml/s

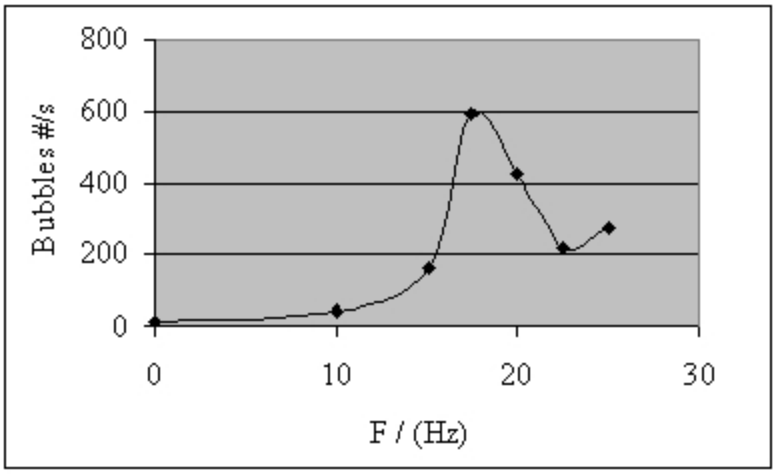

Figure 7. Number of bubbles per sec vs. Frequency
(Direct counting of bubbles leaving 38 mm vertical nozzle
V=0.18 ml/s, nozzle S.G.V = 407.4 mm/s, Cam A = 1.36 mm)

At all low flowrate experimental conditions we have tested (eg. 0 -15ml/s-injector) and desired forcing frequencies (eg. 10 - 30 Hz), we have observed no coalescence of the generated bubbles. We quantified this fact by visually counting bubbles at two cross section locations above the oscillating membrane. The results at both 17.8cm and 36.8cm above the membrane are consistent (and both are consistent with bubble/s counted directly from the injector) and indicate coalescence is not occurring. This fact is another important feature of the forced system.

Krishna et al. (2000) initially used a loudspeaker (flexible piston at the base) to force a single capillary BCR at a very low gas nozzle velocity of 1.35 m/s (0.17ml/s). Bubble numbers show little increase from 0-100 Hz and a steep local maxima approaching 120 bubbles/s near100 and 125 Hz at amplitudes exceeding 2mm. However, the amplitudes indicated by Krishna et al.(2000) seem unlikely from a loudspeaker system. For example, at 50 Hz, the indicated 6mm amplitude on their 5.7 kg water column would require over 3000 Newtons of force. Later, Ellenberger and Krishna (2002); Krishna and Ellenberger (2003) used a solid piston base with electromagnetic vibration to force a single capillary BCR at a gas nozzle velocity of 0.83 m/s (0.528ml/s) and amplitudes ranging from < 0.01mm to 0.32mm. Results showed a linear increase in bubble number with frequency to the first maximum of about 125 bubbles/s again near 100 Hz. At these very low flowrates our results (Figure 7 at 0.407 m/s (0.18 ml/s), and 1.36mm cam amplitude) show a much different result – bubbles/s have reached a first maximum at 17.5 Hz with about 600 bubbles/s. Our results show greater bubble numbers and a lower forcing frequency for the first maximum, compared to Krishna and Ellenberger. The column size used by Krishna was 10 cm while our unit has a diameter of 8.9cm.

By taking high speed photographs of an all glass gas injection system (shown in the next section) we have established the mechanism that caused bubble fragmentation at low flowrates. At low gas flowrates under **unforced** conditions, a suck-back of liquid into the injector is observed after each individual bubble leaves the injector. This is a well-known capillary phenomenon and its effect is reduced as the gas flowrate is increased. Under **forcing** this suck-back is imposed vigorously by the liquid phase oscillations in the column. The suck-back can occur even during bubble formation at the injector tip. The primary mechanism for breakage is as follows. At the time of birth, the bubble and some water are sucked back into the capillary gas feeder tube owing to the backflow phase of the impressed oscillation. Because the forming bubble is forced back into the tube, there is a brief period of slug flow in the capillary. Because the wetted wall diameter is very small, the wall shear is very large, and this stress is greater than the surface tension forces holding the slug intact. The intense shear imposed on the single gas slug causes it to break into many smaller slugs, much as in a drinking straw under high suction. When liquid flow in the column changes to upflow, the many smaller slugs are ejected by the high momentum liquid surrounding the slugs.

Basically the vibrations in the column bottom cause a suck back of the bubble and water into the capillary injection system ultimately creating a “induced shear breakage” of the bubbles. The low frequencies we are using (10 - 30 Hz) has allowed reverse flow into the capillary to occur and the liquid stress deforms the slug giving many smaller slugs.

This elegantly simple and visually verified mechanism, explains much about other work done in the field. We need to undertake further study on the stability of slug flow (Wallis, 1969). There is a critical stability limit for slug flow to be maintained.

The complete mechanism for bubble break-up inside the injector is complex and periodic. Apart from the slug flow regime, bubbly flow and local annular flow has also been observed. Flow inside the injector is highly transient and can undergo continuous regime transitions. Gas bubbles break up inside the injector in broad range of sizes from individual bubbles less than the tube diameter to elongated Taylor-like plugs. Also often during the liquid-ingestion part of the cycle, small bubbles are injected from the neighborhood of the injector tip.

Conditions for reverse flow in the capillary can be ascertained by an elementary force balance. For example, at higher oscillations or low hydrostatic head, reverse flow of the water phase will not occur. In this case bubble breakup at the injector is not expected. The amplitude of the imposed oscillations will also effect this process. This may explain some of the differences between our bubble numbers and the results of others (particularly Krishna and coworkers).

The application of a high speed camera was found to be most useful to study this process. The camera allows the speed and magnitude of bubbles to be determined. Our plan is to initially correlate the observed slug flow behavior and breakup using standard methods (Wallis, 1969). The movement of gas slugs in capillary tubes under pulsed flow conditions has not been studied, to our knowledge. This could be a distinctly separate study.

Photos of Column Operation and Induced Bubble Breakage

To gain a better understanding of the bubble breakup, high speed pictures (Kodak Ektapro Integer Model 1000HRC at 1000 frames per second) using an all glass air injection system were taken. We have performed initial studies to examine the effect of frequency, air flow rate and amplitude. To date, the effect of frequency from 2.5 to 30 Hz (in increments of 2.5 Hz) at several air flow rates has been photographically studied. The pictures below were taken at 17.5 Hz vibration frequency with a gas feed rate of 0.18 ml/sec and a cam amplitude setting of 1.36mm. Here the actual water amplitude, found in Table 4, is 2.46mm. The glass injector is 0.75 mm i.d., and with a vertical length of 38 mm. As shown in the pictures, gas is introduced from the left while the right side of the tee is a dead leg simply used to help support the tee across the column.

The time span between consecutive pictures is 0.001 s. With an external vibration frequency set at 17.5 Hz, about 60 frames were captured for each vibration cycle (1000fps per 17.5 cycle/s ~ 60 frames/cycle). Here, approximately 30 pictures were taken in the upward movement of the membrane and the next 30 pictures were in the downward movement of each vibrating cycle. Below (Figures 8a - 8l) we have chosen pictures every 0.005 seconds to show the entire process starting with the initial suck back at time = 0, and the expulsion phase starting at time = 0.030s.

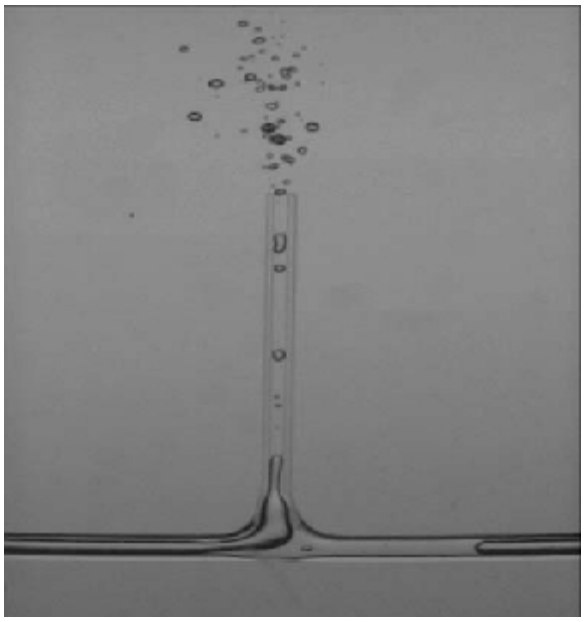

Figure 8a. t = 0
Start of suck back (expulsion completed)

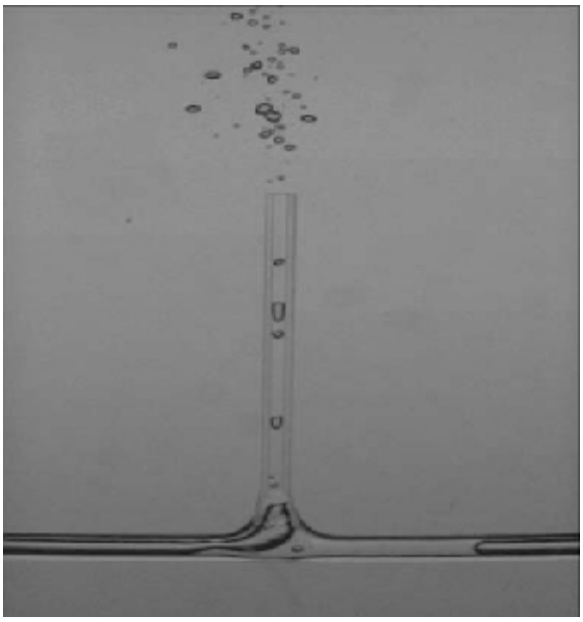

Figure 8b. t = 0.005s
Downward motion of air bubbles in the injector

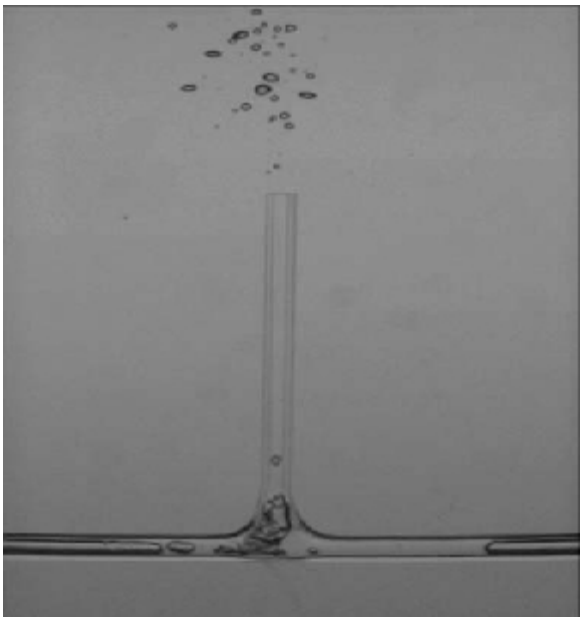

Figure 8c. t = 0.01s
Continued downward movement of the bubbles

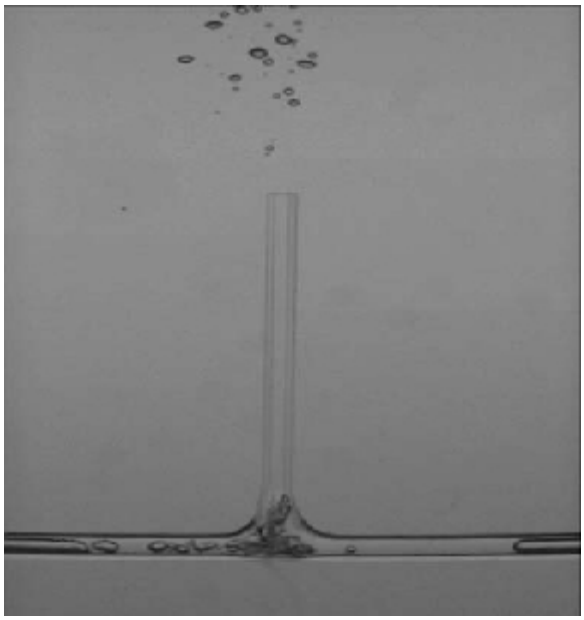

Figure 8d. t = 0.015s

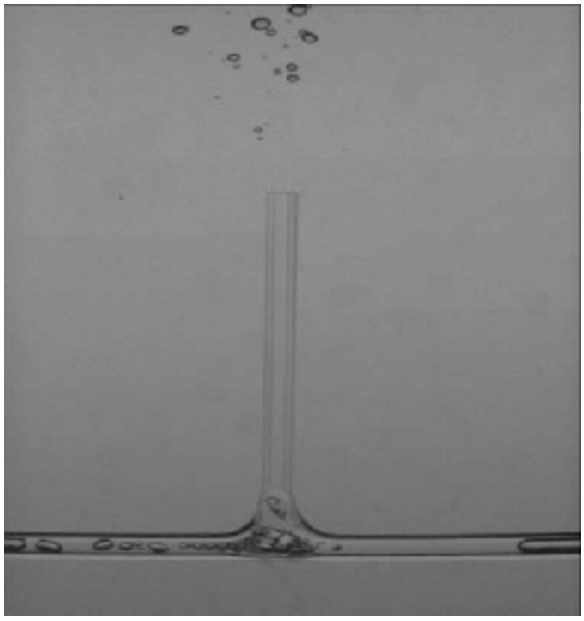

Figure 8e. t = 0.02s

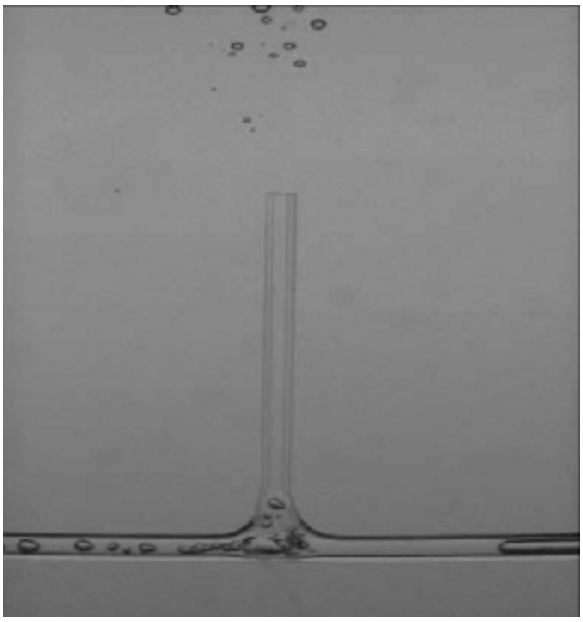

Figure 8f. t = 0.025s
Vertical injector tube completely filled with water

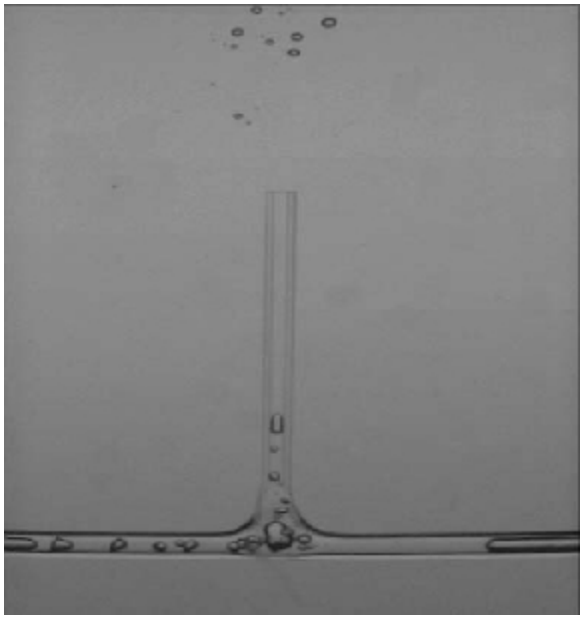

Figure 8g. t = 0.03s
Start of expulsion phase

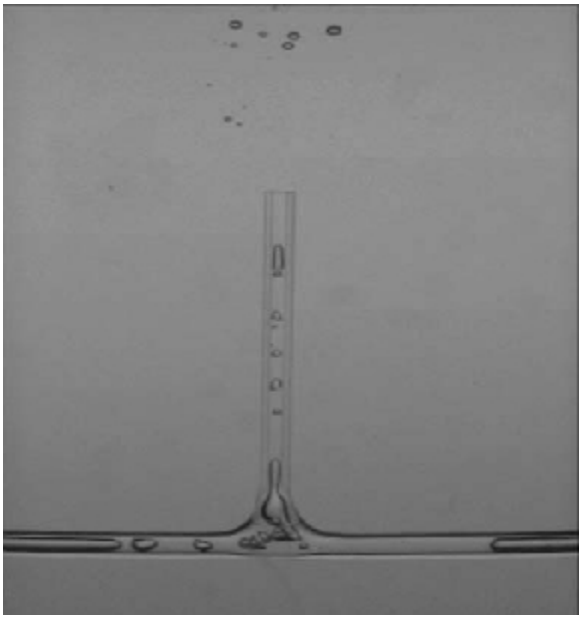

Figure 8h. t = 0.035s
Expulsion of bubbles continues

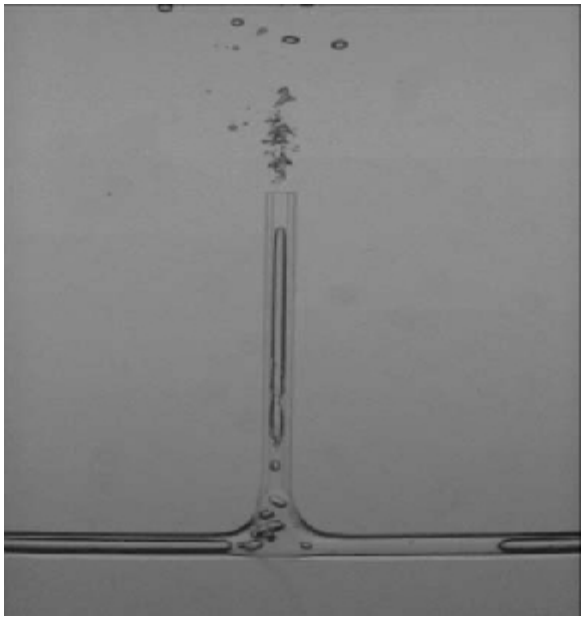

Figure 8i. t=0.04s
High velocity (185 cm/s) of air slug causes additional bubble shearing at nozzle tip

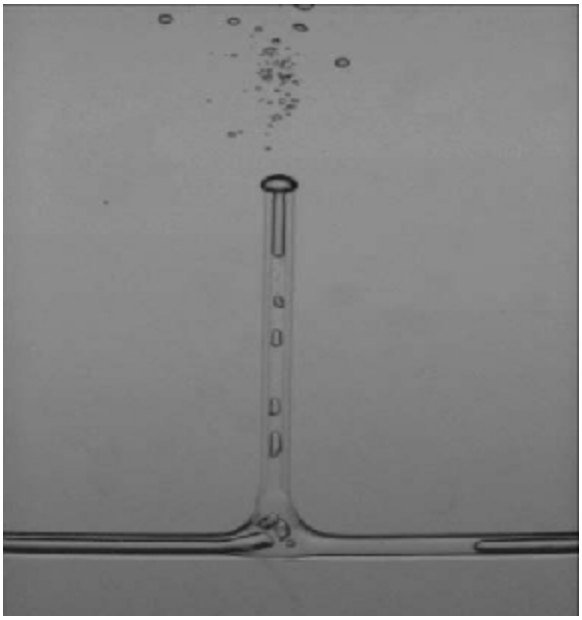

Figure 8j. t = 0.045s
Large bubble forming at nozzle tip

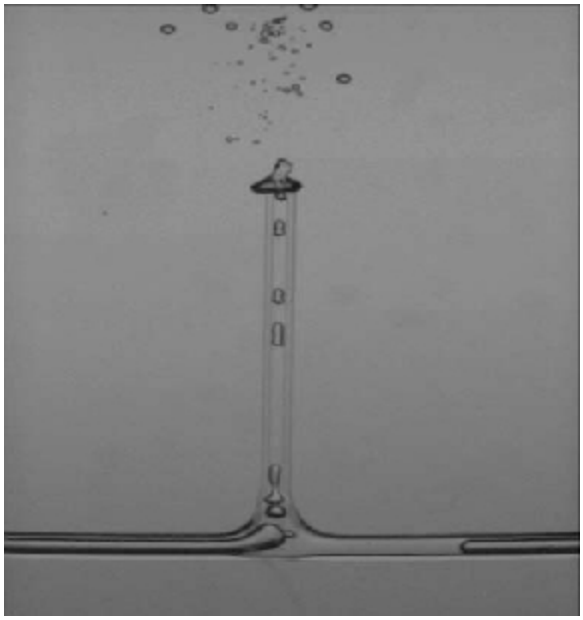

Figure 8k. t = 0.05

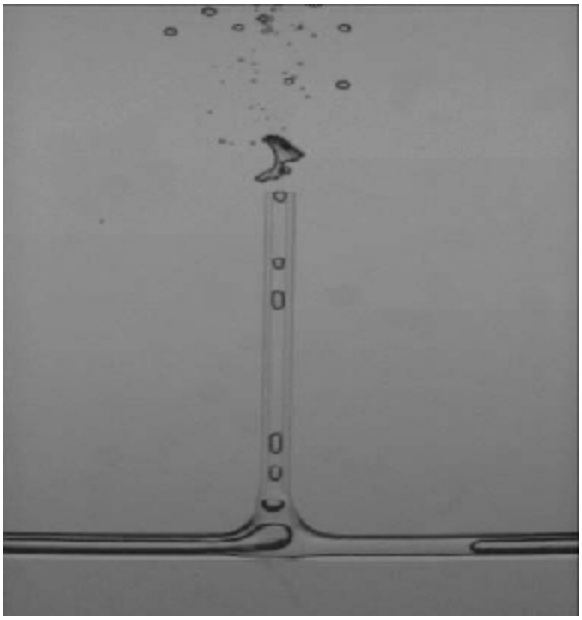

Figure 8l. t = 0.055s
Near end of expulsion process

It is straightforward to use these photographs to determine bubble/s, and bubble size, if desired. For example, the last picture of the cycle shows about 35 new bubbles, which implies (35 bubbles/cycle x 17.5 Hz) 600 bubbles/s. This bubble count is averaged over 15 full cycles before being reported in Figure 3c.

These pictures of the glass injector system clearly show the slug suck-back process, slug instabilities on the injector tube internal wall, and the bubble creation and ejection process. We are apparently the first to observe and report this result. Other researchers (Ellenberger and Krishna (2002); Krishna and Ellenberger (2003); both citing Grinis and Monin (1999)) state bubble breakup occurs at the injector tip (at the orifice) and they attribute the breakup to liquid vibrations which help overcome surface tension forces. Our photographs show a much more complex, but observable mechanism is involved.

Correlation and Modeling of Induced Shear Bubble Breakage

Using the high speed photographs, we were able to determine the average velocity and distance of an air slug, during both the suck back and the expulsion phase, as a function of oscillation frequency. These results are given in Table 6 and plotted in Figure 9.

Table 6: Velocity and distance of air plug movement in capillary injector versus frequency air flowrate 0.18 ml/s, 1.36mm cam amp and 3.18mm rubber sheet

Frequency / (Hz)	Expulsion distance / (cm)	Expulsion velocity / (cm/s)	Suck back distance / (cm)	Suck back velocity / (cm/s)
0	0.29	22.19	0.29	22.19
5	0.41	37	0.41	31.3
7.5	2.22	58.4	2.11	27
10	3.18	79.5	3.37	56.1
12.5	2.81	127.8	2	99.9
15	3.11	182.8	3.03	101.1
17.5	3.33	185	3.03	151.7
20	3.26	171.3	2.66	140.2
22.5	3.14	209.6	2.66	140.2
25	3.14	224.6	3.07	161.6

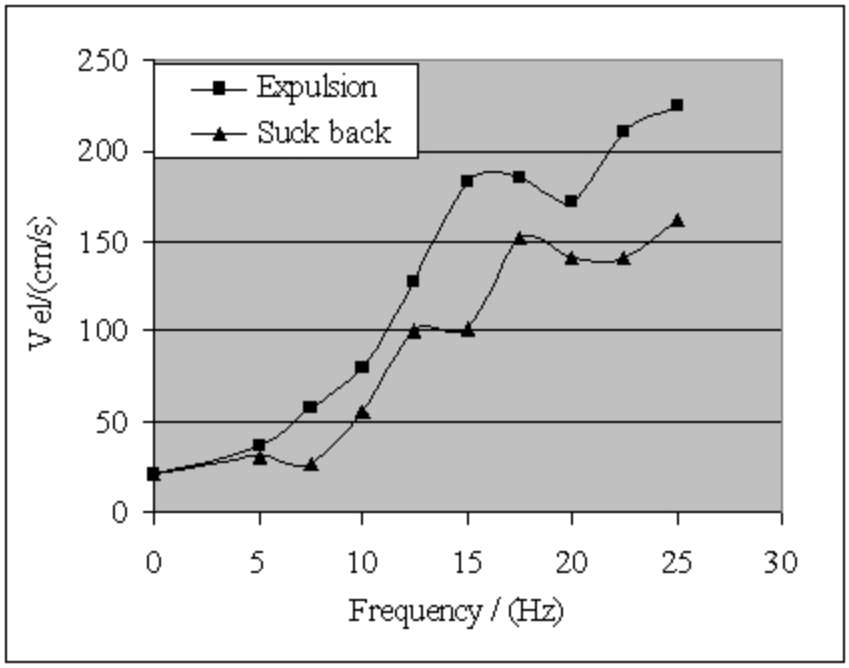

Figure 9. Velocity of expulsion and suck back vs. Frequency
(Cam amplitude = 1.36 mm, V = 0.18 ml/s)

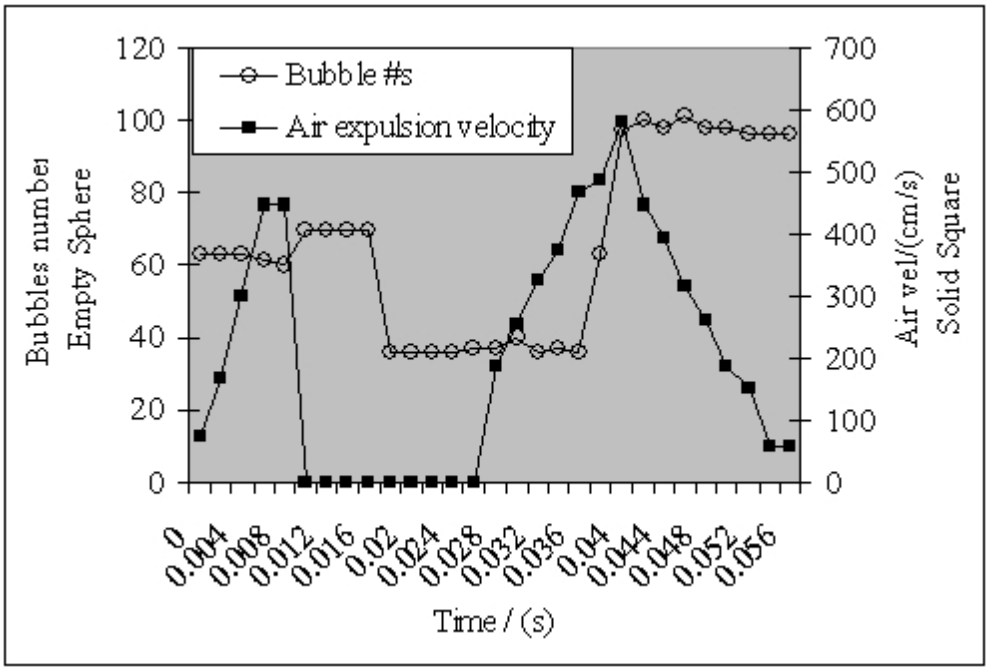

Figure 10a. Relationship of bubbles generation and air slug
expulsion vel. inside of T nozzle at 17.5 Hz

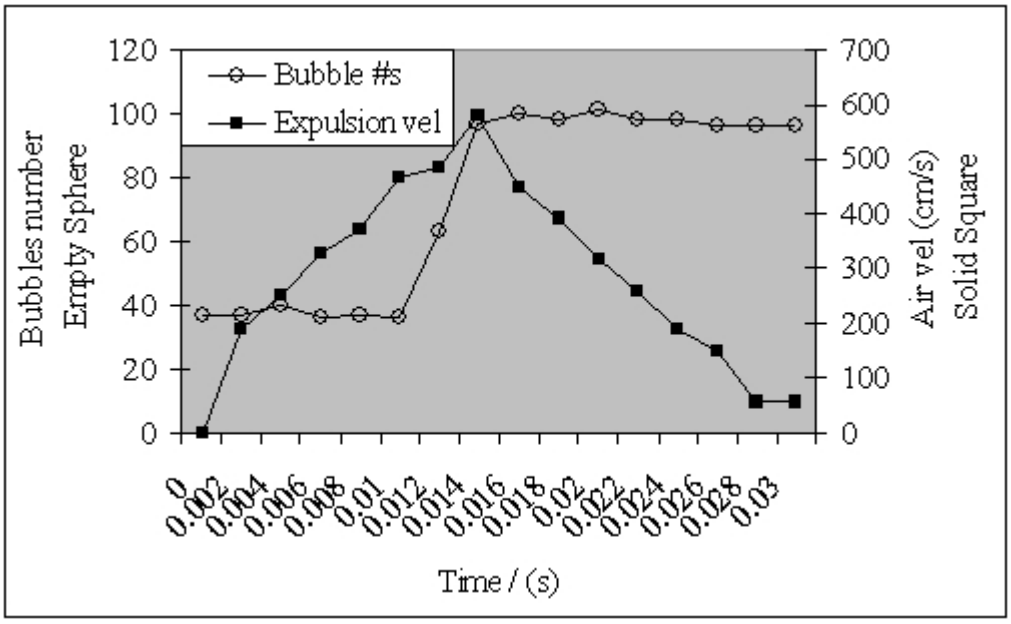

Figure 10b. Relationship of bubbles generation and air slug expulsion vel. inside of T nozzle at 17.5 Hz

Table 6 and Figure 9 provide average velocities which also include a period of zero velocity as flow reversal occurs. It is instructive to examine the instantaneous velocity during the expulsion and suck back cycle. Velocities and number of observable bubbles from the suck back and expulsion cycle shown are given in Figure s 10a and 10b

The highest air slug and corresponding water slug velocity of 600 cm/s produces the largest number of bubbles. At this point an air slug leaving the ejector tip is being impacted by a high momentum water slug. These pictures emphasize the complex mechanism of air slug formation in the feeder tube and high impact water slugs breaking air bubbles at or near the ejector tip (Figure 8).

Mass Transfer and Voidage for Induced Shear Bubble Breakage

We performed experiments to measure the effect of vibration frequency, amplitude and gas volumetric flowrates on both the volumetric mass transfer coefficient and the voidage or gas hold up. For these experiments, a single stainless steel injector (i.d.= 0.75 m; vertical length = 38 m) was used.

The results of a typical oxygen uptake experiment and mass transfer coefficient (k_La) fit are shown in the figure below. In Figure 11, the air flowrate is 1.04 ml/s, giving a nozzle gas velocity of 2.36 m/s and the cam amplitude was 1.36mm and sealing rubber sheet is 3.18 mm

thick. The k_La fit of 0.0008 s^{-1} from equation (6) shows very good agreement with the experimental data.

In Figure 11a below we have plotted measured k_La as a function of frequency for 3 air flowrates (0.51 ml/s; 1.04 ml/s; 2.0ml/s or equivalent nozzle S.G.V. 1.15 m/s; 2.36 m/s; 4.53 m/s) and a cam amplitude of 1.36mm using a 3.18 mm thick membrane. Figure 11a shows that at a cam amplitude setting of 1.36mm, the absolute k_La values increase with increasing flowrate, over the flowrate range tested.

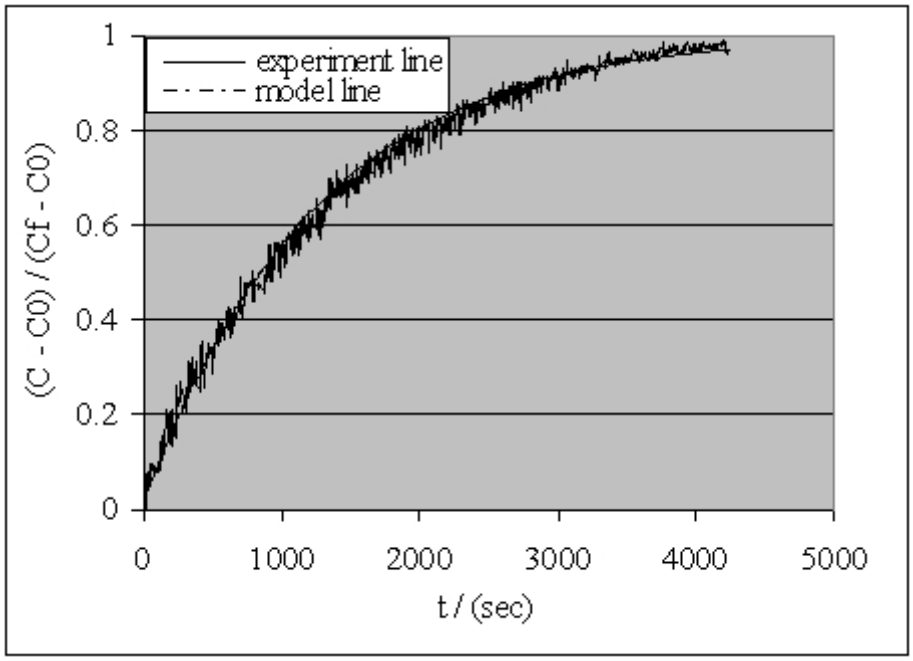

Figure 11. Normalized concentration vs. Time
k_La = 0.0008 s^{-1}, F =17.5 Hz, A = 1.36 mm, V = 1.04 ml/s

For flowrates of 0.51 and 1.04 ml/s, our results show only modest peaks followed by regression to the mean. At 2.0 ml/s, the k_La values actually show a slight linear decrease above 17.5 Hz, as the frequency is increased. These observed trends are emphasized by the non-dimensional k_La (k_La at a given frequency and flowrate / k_La with no forcing at the same flowrate) versus frequency plot in Figure 11b. The k_La enhancement can be substantial; with a flowrate of 2 ml/s and 17.5 Hz forcing, enhancement factors exceeding 2.2 (compared to unforced k_La) are observed.

In another set of k_La experiments, the cam amplitude setting was reduced to 0.51 mm and two flowrates (1.04 and 2.0 ml/s) were again used. The results shown in the Figure 12a below show a different trend; the enhanced behavior is no longer observed. At this 0.51 mm cam amplitude setting k_La versus frequency goes through a maximum at 17.5 and by 30 Hz virtually no improvement in k_La is observed (compared to the unforced case). As shown in Figure 12b, the k_La enhancement at 17.5Hz is less substantial at the lower cam amplitude.

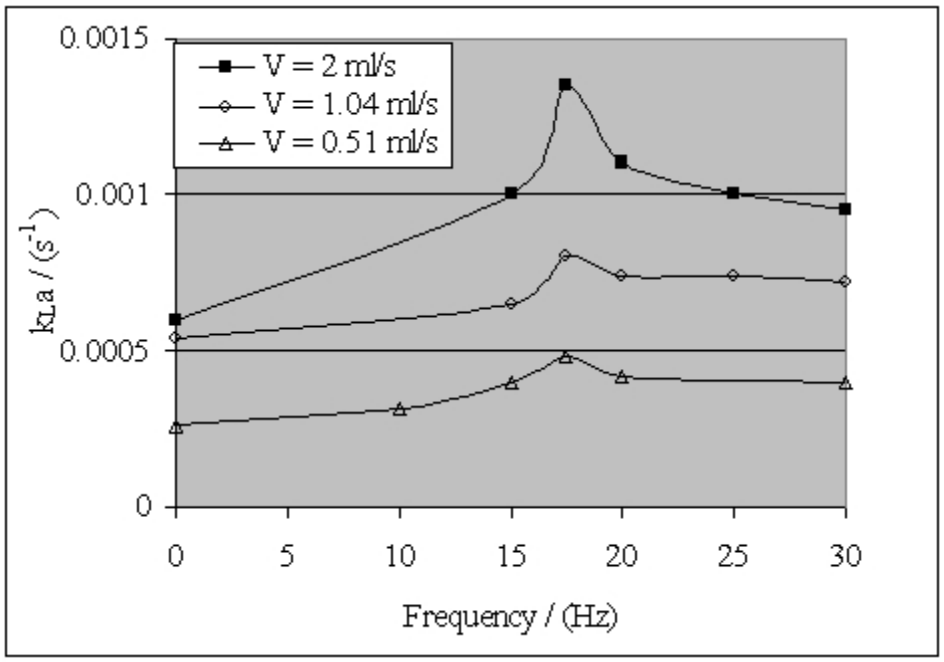

Figure 11a. k_La vs. Frequency - low flowrates
(Cam amplitude = 1.36 mm)

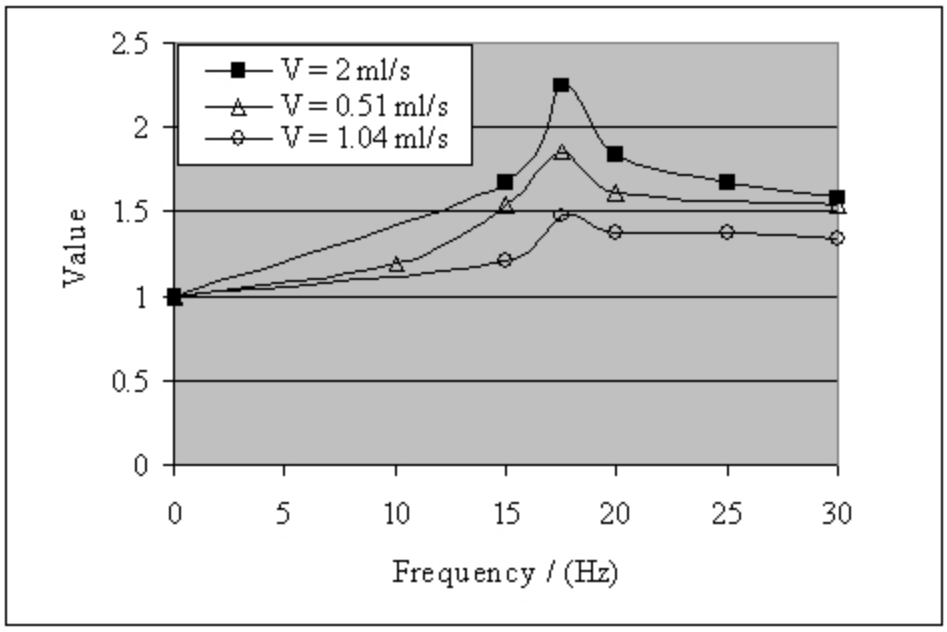

Figure 11b. k_La / k_La (unforced) vs. Frequency
(Cam amplitude = 1.36 mm)

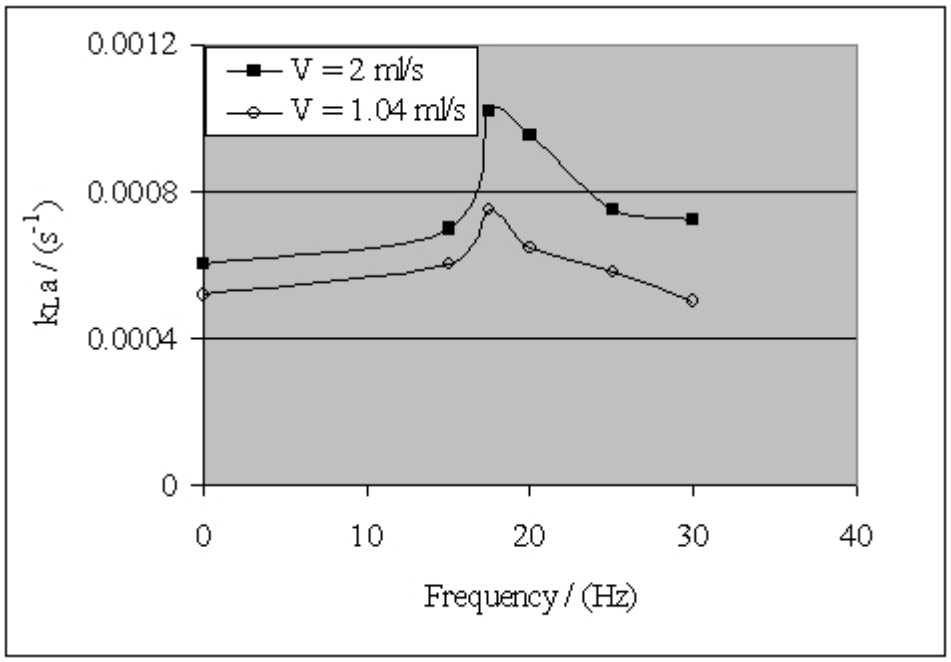

Figure 12a. $k_L a$ vs. Frequency - low flowrates
(Cam amplitude = 0.51 mm)

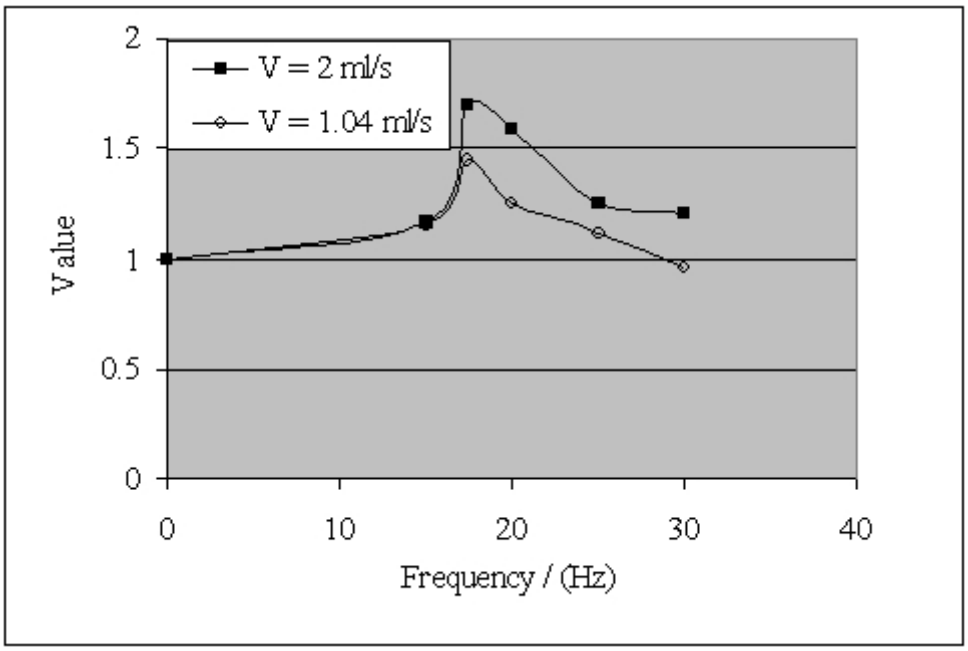

Figure 12b. $k_L a$ /$k_L a$ (unforced) vs. Frequency
(Cam amplitude = 0.51 mm)

These results (Figures 11 and 12) would indicate a complex interaction between frequency, flowrate and cam amplitude. As the frequency increases there is less time for suck back before the expulsion phase begins. At some frequency, the distance of the water suck back will become shorter The cam amplitude setting and gas flowrate will impact the depth of the flow reversal in the injector tube.

It is obvious from Figure12, that the increasing frequency of the flow reversal above 17.5 Hz combined with a "smaller" cam amplitude (0.51mm), led to a lessening of the depth of suck back and slug formation in the injection tube.

Consequently above 17.5 Hz enhanced bubble formation lessens from small to nil. Apparently, by 30 Hz there is no significant suck back of water in the feeder tube at the tested flowrates and the k_La values have returned to unforced values. In contrast, at the higher cam amplitude of 1.36mm there is suck back and bubble generation to 30 Hz. The lessening depth of the suck back with increasing frequency is being counterbalanced by the increased velocity of the suck back and expulsion at this "higher" cam amplitude setting (see figure 9). This combined effect produces the slight decrease in k_La values observed above 17.5 Hz, at the cam amplitude setting of 1.36mm (Figure 11).

These ideas can be verified with high speed photography and an all glass injector system – this work is in progress. It is clear that at some cam setting there will be a gas flowrate where no suck back will be observed.

In fact, at a cam setting of 1.36 mm we have photographically confirmed gas flowrates exceeding 15 ml/s - single injector produce no suck back in the feeder tube. We are currently developing a nonlinear force balance around the injector tip which includes the periodic momentum flux from reverse liquid flow.

The observed trends in k_La versus voidage will be detailed at the end of paper. Voidage measurements are often desired (as opposed to k_La) because they are simple and rapid. Recall voidage measurements consist of simply measuring Δh on a manometer. Voidage measurements below 1.04 ml/s were not possible - the combination of column oscillation and small Δh manometer readings made measurements unreliable. As gas volumetric flowrates become larger, voidage measurements become more reliable. Therefore voidage measurements were only arranged at the volumetric flowrates above 1.04 ml/s.

Resonate Bubble Breakage

Resonate column bubble breakage is a mechanism different from the previously discussed induced shear bubble breakage. As the gas flowrate through a single nozzle is increased to values above 15ml/s (nozzle S.G.V 34 m/s, column S.G.V. 0.00241 m/s), induced shear bubble breakage in the injector no longer occurs, however, a resonate frequency bubble breakage occurs as shown in the photographs below (Figure 13).

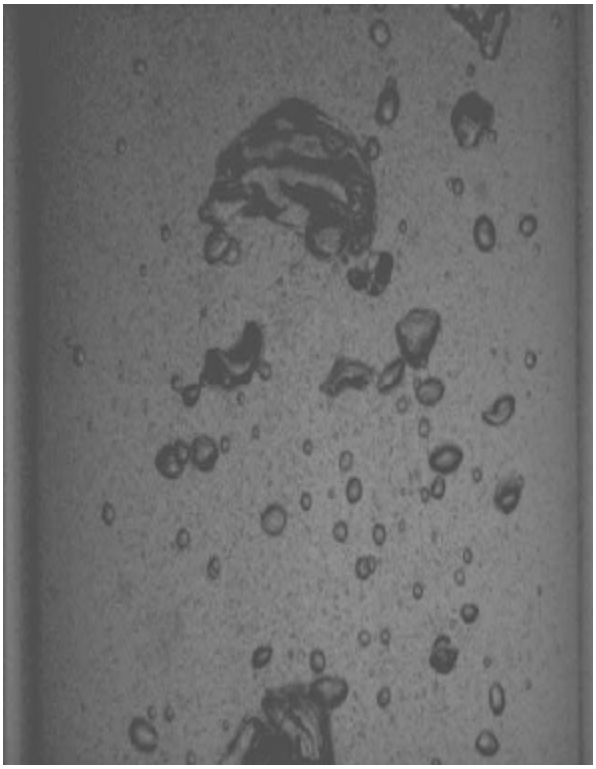

Figure 13a.
Taken 350 mm above nozzle outlet
No forcing
V = 36.4 ml/s

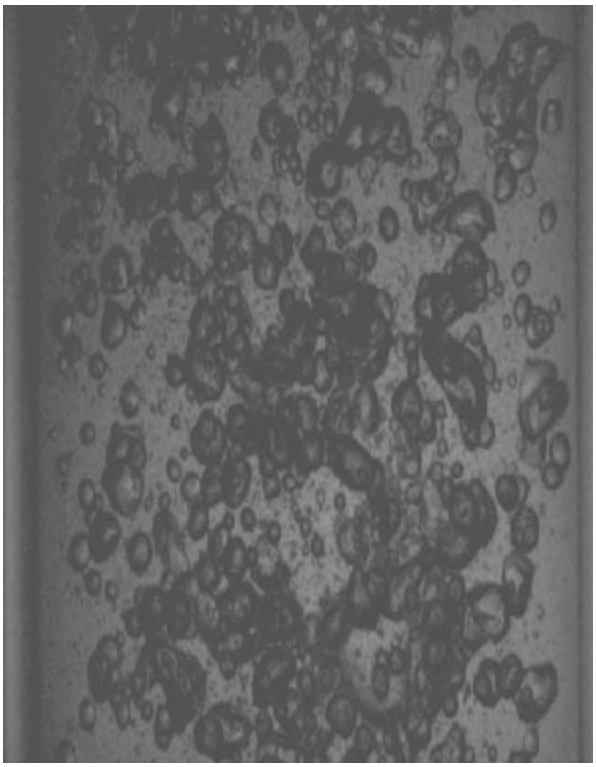

Figure 13b.
Taken 350 mm above nozzle outlet
Forcing frequency = 16 Hz
Cam amplitude 1.36 mm
V = 36.4 ml/s

Under conditions of gas high flow and jetting at the injector, bubbles are not individually formed, but arise from jet break-up. These large bubbles are easily fragmented by the intense shear caused by flow reversal in the liquid phase. As previously detailed, induced shear breakage occurs as a result of water suck back in the gas feeder tube. This suck-back creates wetted walls which enhance shearing of the gas slugs during the expulsion phase.

In addition some air and water slugs form in the feeder tube and their interactions promotes bubble formation in the tube. This observed phenomena occurs at relatively low flowrates which are normally associated with bubbly flow. At a cam amplitude of 1.36 mm we have observed suck back to nozzle gas velocities of about 30 m/s. Above these velocities, jet flow is observed with no flow reversal. This is easy to understand; at any given cam amplitude a gas flow can be obtained which simply "overpowers" the reverse flow created by the column forcing.

At these higher gas volumetric flowrates (above 30 m/s), an entirely different mechanism has been observed which leads to dramatic improvements in column operation; here improvements well above the 50 to 120% owing to induced shear bubble breakage are possible. Normally at

these higher jet volumetric flowrates, "globs" of air leave the injector. This is typical of an industrial mode of operation where it is often believed – more is better – the more gas that can be forced into the column the better the column performance. Of course there are notable exceptions, including fermentation, where high flowrates are not used as they could damage sensitive organisms.

It is important to note that at all high volumetric flowrate experimental conditions we have tested (eg. 15 -35 ml/s-injector) and desired forcing frequencies (eg. 10 - 30 Hz), we have again observed no coalescence of the generated bubbles. The generated bubbles fill the available column (see photographs at the start of the section) – there has been no observed flow bias toward the column center. These results agree with those we found with lower volumetric flowrates.

Mass Transfer and Voidage for Resonant Bubble Breakage - Flexible Piston

We again performed experiments to measure the effect of vibration frequency, vibration amplitude and gas volumetric flowrate on both the volumetric mass transfer coefficient and the voidage or gas hold up. For these experiments, a single stainless steel injector (i.d.=0.75 mm; o.d. = 1.5 mm; vertical length=38 mm) was used. The nozzle gas superficial velocities used were 33.9 m/s, 45.3 m/s, 56.6 m/s and 68.8 m/s (or 15 ml/s, 20 ml/s, 25 ml/s, and 30.4 ml/s in gas volumetric flowrates), through the single nozzle. Cam amplitudes of both 1.36mm and 0.51 mm were tested with rubber sheets of 3 different thicknesses (1.59 mm (1/16"); 3.18 mm (1/8"); 6.35 mm (1/4")).

The tables (7 and 8) and Figures (14 and 15) below summarize results for **one** high gas flowrate of 30.4 ml/s. The plot of k_La versus frequency for the 3.18 mm (1/8") rubber sheet in Figures 14b and 15b show a dramatic behavior. The k_La values go through a steep symmetric maximum at about 17.5Hz. Figure 14b shows the k_La enhancement is about 225% (compared to the unforced values).

Also in Figure 14b, normalized amplitude measurements seem to coincide with the normalized k_La values, however, voidage enhancements are not as large as observed for k_La. Figure 15b shows different results for these same conditions, with a lower cam amplitude setting of 0.51mm. Here the normalized amplitudes are much larger than normalized k_La values which in turn are again larger than the normalized voidage values. Figure 15b also shows the frequency maximum in amplitude is shifted, compared to the frequency maximum in k_La or voidage.

In tables 7 and 8 we have also indicated if sloshing was observed. As discussed in a later section, Applying the Benjamin and Ursell Stability Theory to Resonate Bubble Breakage, sloshing indicates an unstable region of BCR operation. This surface instability is inextricably linked to an increased mass transfer coefficient.

Table 7a: Cam amp 1.36 mm, membrane 1.59 mm and V=30.4 ml/s, A_0 = 0.74 mm

F (Hz)	A (mm)	A/A0	Voidage	N-Voidage	Sloshing
0	0.74	1	0.0113	1	N
10	0.52	0.70	0.0122	1.08	N
15	**1.69**	2.28	0.0223	1.97	**Y**
17.5	**1.66**	2.24	0.0141	1.24	**Y**
20	0.97	1.31	0.0115	1.02	N
22.5	0.78	1.05	0.0114	1.00	N
25	0.71	0.96	0.0113	1.00	N
30	0.39	0.53	0.0112	0.99	N

F (Hz)	k_La	N-k_La
0	0.004	1
15	0.012	3
17.5	0.0085	2.125

Table 7b: Cam amp 1.36 mm, membrane 3.18 mm and V=30.4 ml/s, A_0 = 0.74 mm

F (Hz)	A (mm)	A/A0	Voidage	N-Voidage	Sloshing
0	0.74	1	0.0113	1	N
10	0.65	0.88	0.0115	1.02	N
15	1.30	1.76	0.0121	1.07	**Y**
17.5	**2.46**	3.32	0.0208	1.84	**Y**
20	1.69	2.28	0.0135	1.20	**Y**
22.5	1.17	1.58	0.0114	1.01	**Y**
25	1.04	1.41	0.0107	0.95	N
30	0.32	0.43	0.0106	0.94	N

F (Hz)	k_La	N-k_La
0	0.004	1
10	0.004	1
15	0.0067	1.675
17.5	0.013	3.25
20	0.01	2.5
22.5	0.008	2
25	0.006	1.5

Table 7c: Cam amp 1.36 mm, membrane 6.35 mm and V=30.4 ml/s, A_0 = 0.74 mm

F (Hz)	A (mm)	A/A0	Voidage	N-Voidage	Sloshing
0	0.74	1	0.0114	1	N
10	0.78	1.05	0.0116	1.01	N
15	0.84	1.14	0.0140	1.22	N
17.5	1.23	1.66	0.0260	2.27	**Y**
20	1.69	2.28	0.0233	2.04	**Y**
22.5	**1.94**	2.62	0.0159	1.39	**Y**
25	1.81	2.45	0.0131	1.14	**Y**
30	1.1	1.49	0.0108	0.94	N

F (Hz)	k_La	N-k_La
0	0.004	1
17.5	0.012	3
20	0.0132	3.3
22.5	0.0125	3.125

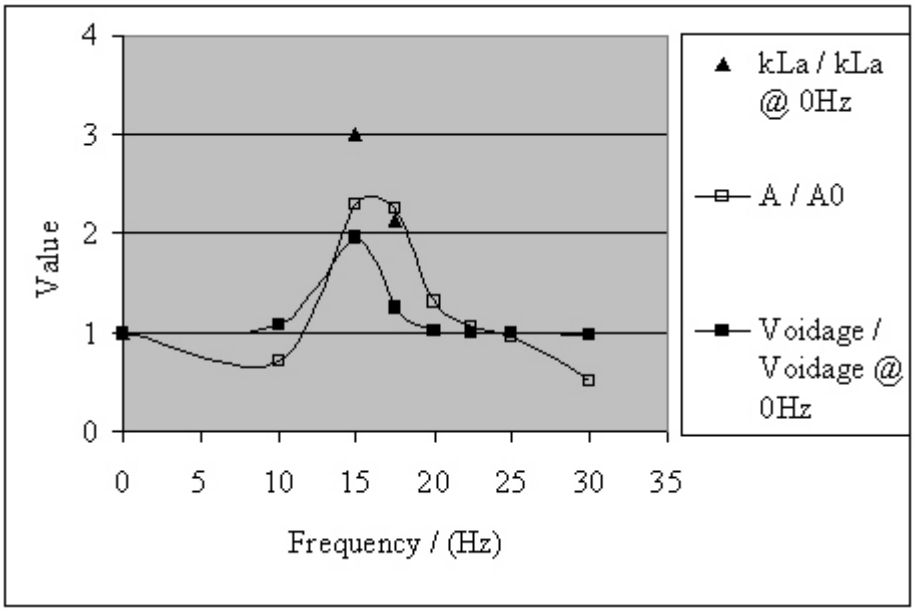

Figure 14a. Normalized k_La, Amp and Voidage vs. Frequency
Membrane 1.59 mm and cam amp 1.36 mm, V = 30.4 ml/s

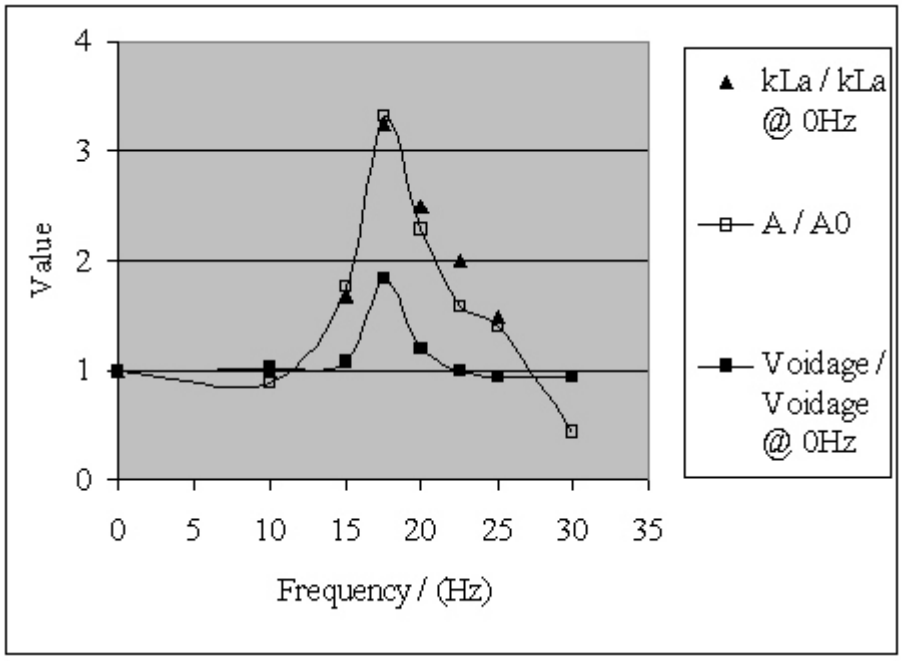

Figure 14b. Normalized k_La, Amp and Voidage vs. Frequency
Membrane 3.18 mm and cam amp 1.36 mm, V = 30.4 ml/s

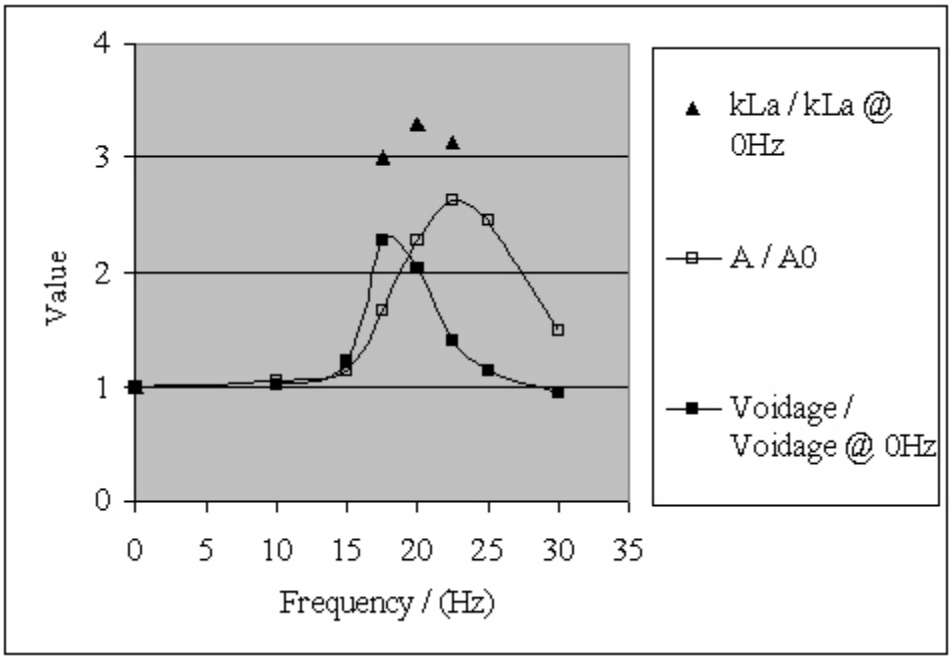

Figure 14c. Normalized k_La, Amp and Voidage vs. Frequency
Membrane 6.35 mm and cam amp 1.36 mm, V = 30.4 ml/s

Table 8a: Cam amp 0.51 mm, membrane 1.59 mm and V=30.4 ml/s, A_0 = 0.303 mm

F (Hz)	A (mm)	A/A0	Voidage	N-Voidage	Sloshing
0	0.303	1	0.0109	1	N
10	0.38	1.25	0.0112	1.03	N
15	0.92	3.04	0.0125	1.15	N
17.5	**1.15**	3.80	0.0131	1.20	**Y**
20	0.61	2.01	0.0125	1.15	N
22.5	0.38	1.25	0.0109	1.01	N
25	0.31	1.02	0.0111	1.02	N
30	0.31	1.02	0.0107	0.99	N

F (Hz)	k_La	N-k_La
0	0.004	1
17.5	0.005	1.25

Table 8b: Cam amp 0.51 mm, membrane 3.18 mm and V=30.4 ml/s, A_0 = 0.303 mm

F (Hz)	A (mm)	A/A0	Voidage	N-Voidage	Sloshing
0	0.303	1	0.0106	1	N
15	0.52	1.72	0.0110	1.04	N
17.5	0.84	2.77	0.0140	1.32	**Y**
20	**1.56**	5.15	0.0107	1.01	**Y**
22.5	0.91	3.00	0.0094	0.89	N
25	0.39	1.29	0.0093	0.88	N
30	0.13	0.43	0.0089	0.84	N

F (Hz)	k_La	N-k_La
0	0.004	1
15	0.0054	1.35
17.5	0.0095	2.375
20	0.0056	1.4
25	0.0048	1.2

Table 8c: Cam amp 0.51 mm, membrane 6.35 mm and V=30.4 ml/s, A_0 = 0.303 mm

F (Hz)	A (mm)	A/A0	Voidage	N-Voidage	Sloshing
0	0.303	1	0.0113	1	N
10	0.38	1.25	0.0122	1.08	N
15	0.31	1.02	0.0135	1.19	N
17.5	0.46	1.52	0.0140	1.24	N
20	0.61	2.01	0.0153	1.35	**Y**
22.5	0.92	3.04	0.0119	1.05	**Y**
25	**1.37**	4.52	0.0115	1.02	**Y**
30	0.46	1.52	0.0112	0.99	N

F (Hz)	k_La	N-k_La
0	0.004	1
17.5	0.005	1.25
20	0.008	2
22.5	0.008	2

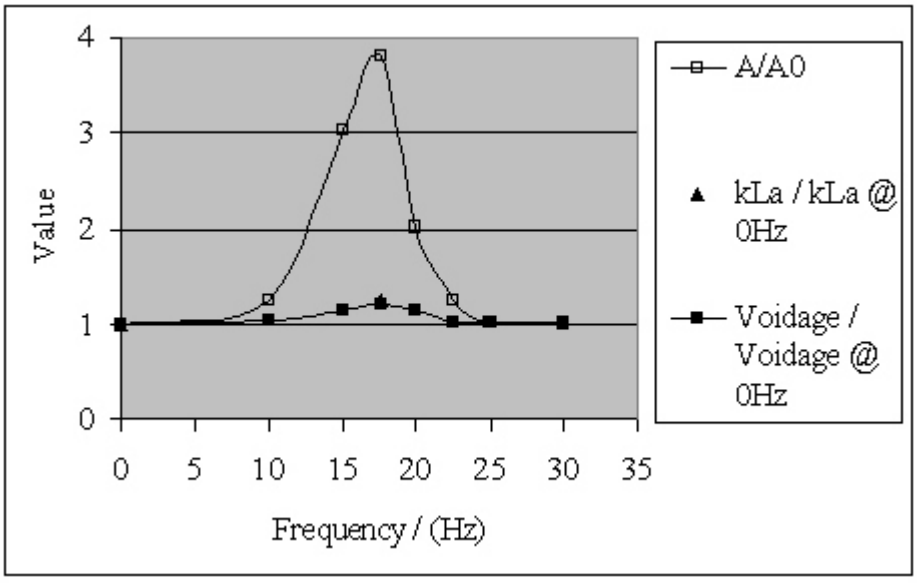

Figure 15a. Normalized k_La, Amp and Voidage vs. Frequency
Membrane 1.59 mm and cam amp 0.51 mm, V = 30.4 ml/s

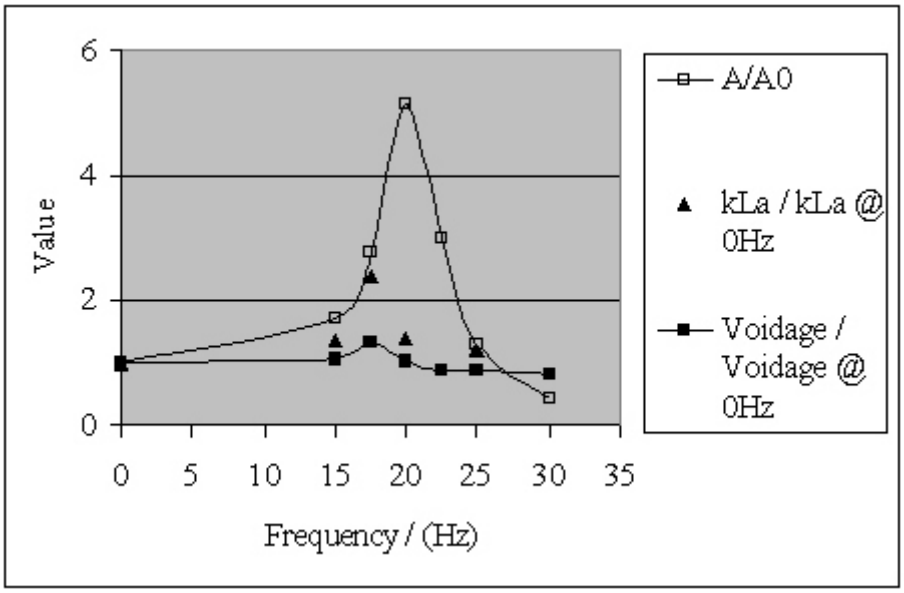

Figure 15b. Normalized k_La, Amp and Voidage vs. Frequency
Membrane 3.18 mm and cam amp 0.51 mm, V = 30.4 ml/s

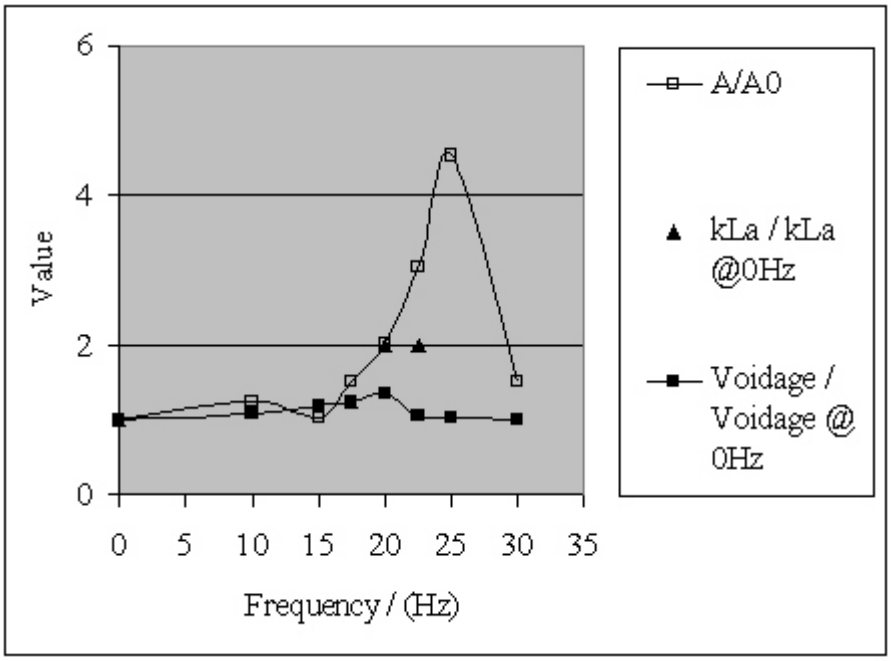

Figure 15c. Normalized k_La, Amp and Voidage vs. Frequency
Membrane 6.35 mm and cam amp 0.51 mm, V = 30.4 ml/s

It is very interesting to observe the effect of changing the thickness of the flexible rubber sheet which acts as a piston at the base of the vibrating bubble column. Using a thinner rubber membrane (1.59 mm), the maximums in voidage, amplitude and $k_L a$ (Figures 14a and 15a) generally shift to a lower frequency (compared to the 3.18 mm thickness rubber sheet). When using a thicker rubber sheet (Figures 14c and 15c) these measured parameters shift to a higher frequency.

This result is expected from the simple model (equation 8) which shows the natural frequency of the system depends on $\sqrt{k}$; the larger the k (thicker) the higher the natural frequency. At the lower cam setting (0.51 mm) normalized amplitudes are again much larger than normalized $k_L a$ values (Figure 15) which in turn are larger than normalized voidage values. In Figures 14 and 15 the frequency for the maximum voidage is generally less than the frequency for the maximum amplitude.

To help clarify these findings we carefully examined the effect of flowrate using the 3.18 mm (1/8") thickness rubber sheet at the two cam amplitude settings of 1.36 and 0.51 mm. The $k_L a$ values go through a steep symmetric maximum at about 17.5Hz at the two cam amplitude settings of 1.36 mm (Figure 14b) and 0.51mm (Figure 15b). This maximum appears to be independent of tested nozzle gas superficial velocities at the tested cam amplitude settings (Figures 16 and 17).

At 17.5 Hz, $k_L a$ enhancements exceeding 200% were found for all tested high flowrates high cam setting (Figure 16b), and $k_L a$ enhancements exceeding 100% were found for tested flowrates at the lower cam setting (Figure 17b).

Voidage measurements versus frequency at 2 different high flowrates and 2 cam settings (Figures 18 and 19) show a maximum at 17.5 Hz, however, the voidage enhancements are not as large as observed for $k_L a$.

It is possible to make some general comments about Figures 14 - 19. In general voidage versus frequency peaks before liquid amplitude versus frequency. A possible reason for this is as follows: when amplitude starts its run up with increasing frequency, bubble breakage occurs, usually with second order kinetics, meaning two bubbles form from one large one. This of course increases voidage. More breakage occurs as frequency increases until a critical bubble size occurs.

Beyond this point, bubbles no longer break. Bubbles may actually be thrown together so intensely that coalescence occurs which causes voidage decrease even though the observed amplitude is still increasing.

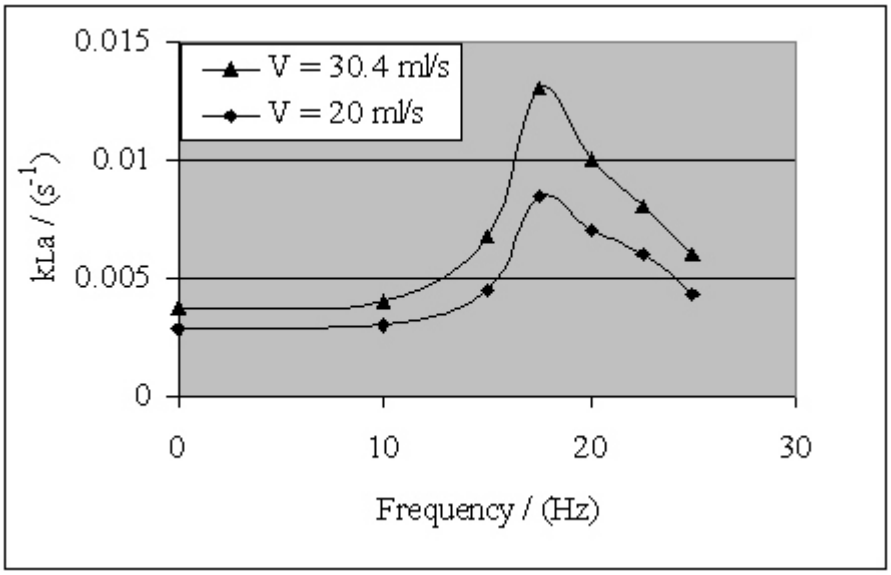

Figure 16a. k_La vs. Frequency (Cam amplitude = 1.36 mm)

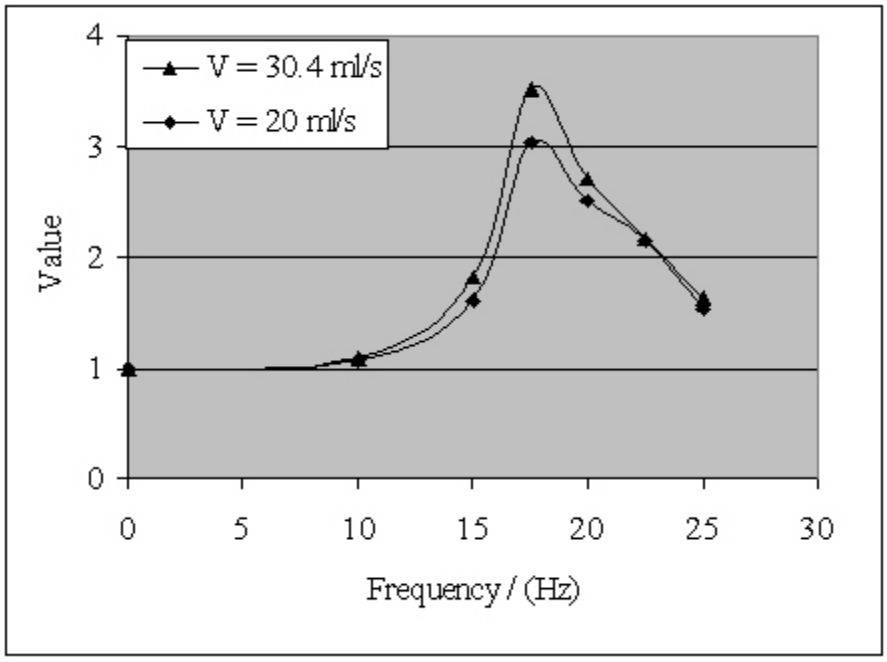

Figure 16b. k_La / k_La (unforced) vs. Frequency
(Cam amplitude = 1.36 mm)

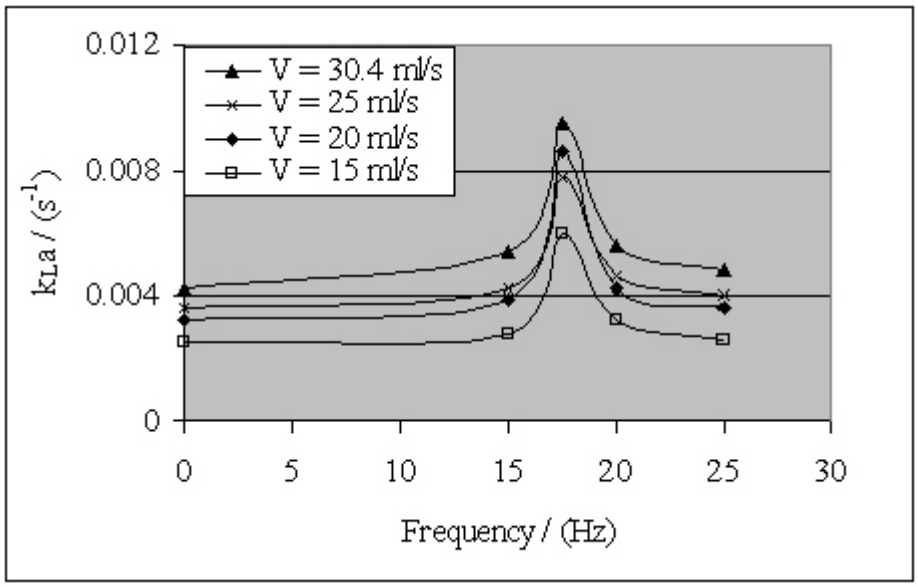

Figure 17a. k_La vs. Frequency (Cam amplitude = 0.51 mm)

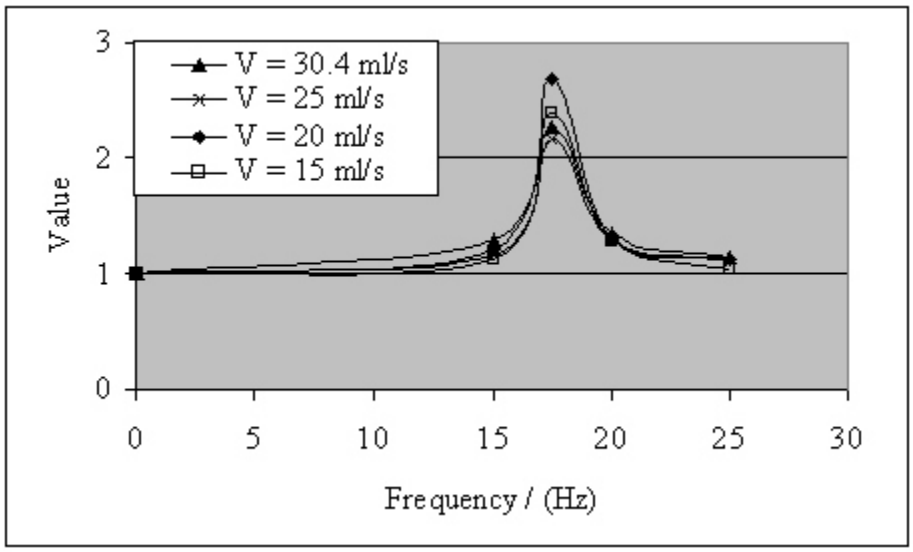

Figure 17b. k_La / k_La (unforced) vs. Frequency
(Cam amplitude = 0.51 mm)

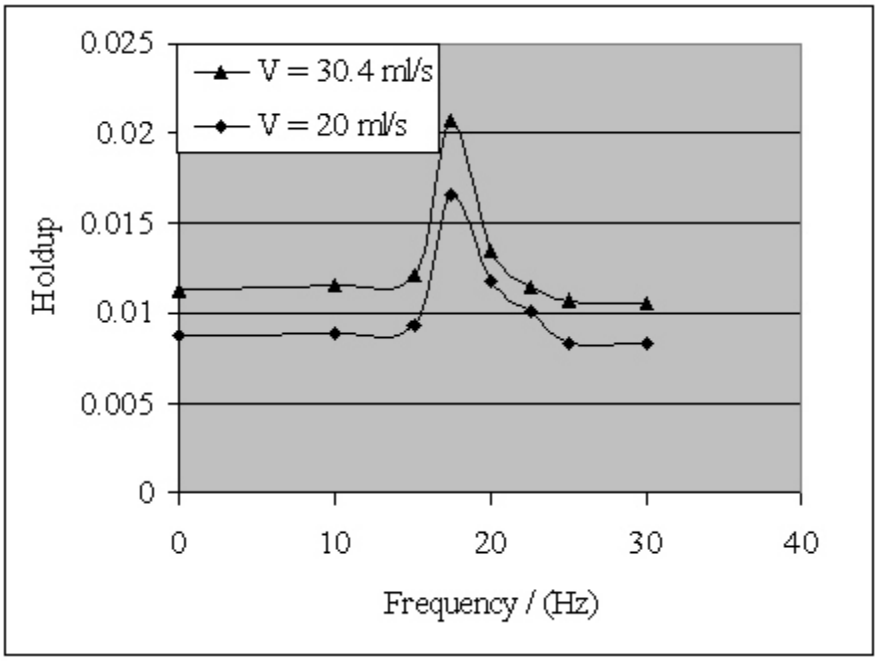

Figure 18a. Air holdup vs. Frequency
(Membrane 3.18 mm and cam amplitude = 1.36 mm)

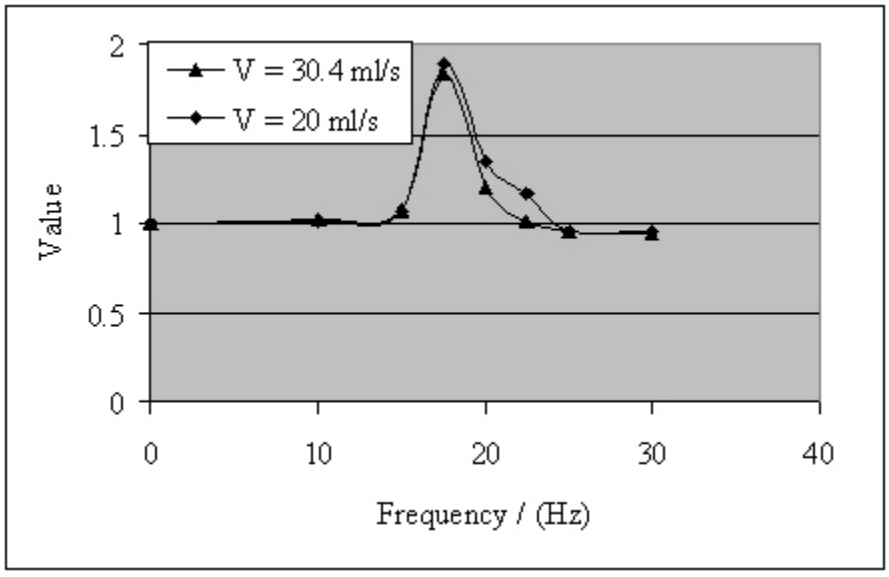

Figure 18b. Holdup / holdup (unforced) vs. Frequency
(Membrane 3.18 mm and cam amplitude = 1.36 mm)

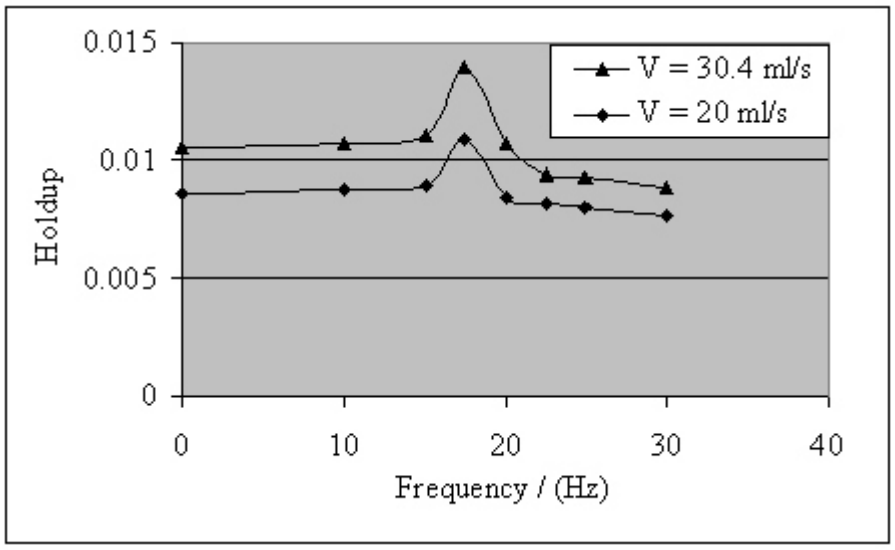

Figure 19a. Air holdup vs. Frequency
(Membrane 3.18 mm and cam amplitude = 0.51 mm)

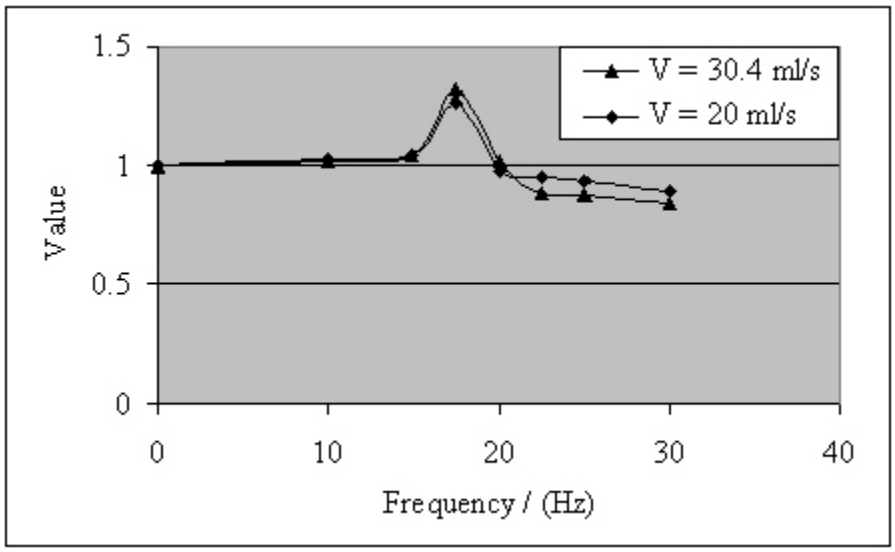

Figure 19b. Holdup / holdup (unforced) vs. Frequency
(Membrane 3.18 mm and cam amplitude = 0.51 mm)

Mass Transfer and Voidage for Resonant Bubble Breakage - Solid Piston

To create a solid piston, the natural gum rubber sheet (3.18 mm) at the base of the column is clamped between 2 stainless steel disks each 8.26 cm in diameter. The column diameter is

8.9 cm, which allows oscillation of a maximum of 2.74 cm^2 of rubber at the column base; this is really just a comfortable wall clearance for the metal disks. The k_La enhancements, for different fixed amplitudes of the solid piston, at our maximum flowrate of 30.4 ml/s are given in Table 9 and plotted in Figure 20a.

The first analysis is to compare the k_La enhancements, obtained for the same amplitude and frequency, from both the flexible piston and the solid piston; the enhancements were expected to be the same. This is done in Figure 20b. Here the curved lines represent the solid piston results, the actual data points for the solid piston have been omitted for clarity. The data points that are shown in Figure 20b are from the flexible piston using Tables 7 and 8 where the amplitudes and frequencies are near solid piston conditions. In general, the k_La enhancements from the flexible piston and solid piston base show good agreement at lower frequencies and lower amplitudes. For example, at 1.66 mm amplitude and 15 hz the k_La enhancement is 2.75 (Table 9b) compared to similar conditions in Table 7a with a k_La enhancement of 3. At 1.23 mm amplitude and 17.5 hz the k_La enhancement is 2.75 (Table 9c) compared to these same conditions in Table 7c with a k_La enhancement of 3. At 0.84 mm amplitude and 17.5 hz the k_La enhancement is 2 (Table 9d) compared to these same conditions in Table 8b with a k_La enhancement of 2.38.

However as the amplitude and frequency increase, there is less agreement between the solid piston results and the flexible piston results. The k_La enhancements are larger with the solid piston base at high tested amplitudes and higher frequencies. For example, Table 9a shows at 2.46 mm amplitude and 17.5 hz the k_La enhancement is 6.25 compared to these same conditions in Table 7b with a k_La enhancement of 3.25. At 1.66 mm amplitude and 20 hz the k_La enhancement is 6.00 (Table 9b) compared to similar conditions in Table 7b and c with k_La enhancements of 2.5 and 3.3. One explanation may be that at higher frequencies and amplitudes, the small area of rubber (a maximum of 2.74 cm^2 of rubber) at the column base may be causing increased amplitudes as observed with the flexible piston. We will need to experimentally verify this fact. For example, we observed at 2.46mm amplitude and 15hz (Table 9a), the bubble pattern and column surface appeared similar to column performance at 17.5hz (Table 7b) with the flexible piston. One can compare the k_La enhanced values at 3.5 (Table 9a) and 3.25 (Table 7b). As will be discussed below the column free surface provides a strong indication of column performance (k_La enhancement), since instability at the surface portends unstable flow close beneath the surface.

The solid piston results are astounding. Enhancements in k_La in excess of 500% are observed with 2.46 mm amplitude and frequencies as low as 17.5 hz. Enhancements in excess of 400% are possible with amplitudes as low as 1.23 mm and frequencies as low as 20 hz. These enhancements far exceed previously reported values, in this or any published manuscript. It is possible to make some general comments about Figure 20a. At constant amplitude, as the frequency increases, bubble breakage increases. This will usually occur with second order kinetics, meaning two bubbles form from one large one. More breakage occurs as frequency increases until a critical bubble size occurs. Beyond this point, bubbles no longer break. The new surfaces created during breakage cause big increases in k_La, and after the critical bubble size is

reached, no further increase is possible. This explains the run up in mass transfer coefficient values reaching a plateau. This plateau phenomenon was not observed with the flexible piston because of the dynamic phase shift effects in the rubber - the amplitude reached a maximum and quickly dropped off.

Table 9: Membrane 3.18 mm, solid piston, V=30.4 ml/s

a) Piston amp 2.46 mm

F (Hz)	k_La	N-k_La	Slosh/ foam
0	0.004	1	N
10	0.006	1.5	N
12.5	0.0085	2.125	N
15	0.014	3.5	S
17.5	0.025	6.25	F
20	0.025	6.25	F
25	0.025	6.25	F

b) Piston amp 1.66 mm

F (Hz)	k_La	N-k_La	Slosh /foam
0	0.004	1	N
10	0.0065	1.625	N
15	0.011	2.75	S
17.5	0.018	4.5	S
20	0.024	6	F
22.5	0.0235	5.875	F
25	0.022	5.5	F
30	0.024	6	F

c) Piston amp 1.23 mm

F (Hz)	k_La	N-k_La	Slosh /foam
0	0.004	1	N
10	0.0056	1.4	N
15	0.0078	1.95	N
17.5	0.011	2.75	S
20	0.02	5	F
22.5	0.019	4.75	F
25	0.02	5	F
30	0.02	5	F

d) Piston amp 0.84 mm

F (Hz)	k_La	N-k_La	Slosh /foam
0	0.004	1	N
10	0.0052	1.3	N
15	0.006	1.5	N
17.5	0.008	2	S
20	0.011	2.75	S
25	0.0168	4.2	F
30	0.017	4.25	F

e) Piston amp 0.46 mm

F (Hz)	k_La	N-k_La	Slosh /foam
0	0.004	1	N
10	0.0048	1.2	N
15	0.0052	1.3	N
17.5	0.0052	1.3	N
20	0.0054	1.35	N
22.5	0.0065	1.625	N
25	0.0092	2.3	N
30	0.016	4	F

We also observed column foaming at some conditions (Table 9). Here with the solid piston at high amplitudes and frequencies, smaller bubbles are moved so violently that the surfaces are cleansed (removing surfactant film) and allowing recoalescence, thereby reducing voidage. During the run up period, enhancement occurred mainly from increased “a”, but also owing to surface renewal by giving birth to new, smaller bubbles. This process continues as frequency

and/or amplitude is increased until a critical, minimum bubble size is attained. Increases in frequency or amplitude beyond this serves only to cleanse the bubble surface, and at some point, bubble coalescence between cleaned bubbles can arise, which serves to reduce voidage. The penetration of the boundary layer around the moving bubbles can be linked to the energy dissipation in the system, which increases with frequency and amplitude.

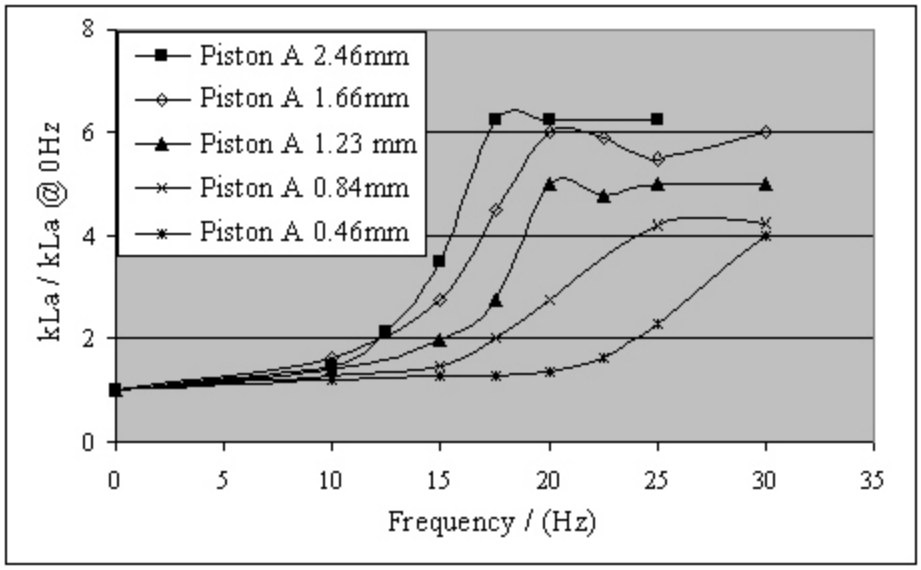

Figure 20a. k_La/k_La @ 0 Hz vs. Frequency
Membrane 3.18 mm solid piston O.D. = 8.355 cm and V = 30.4 ml/s

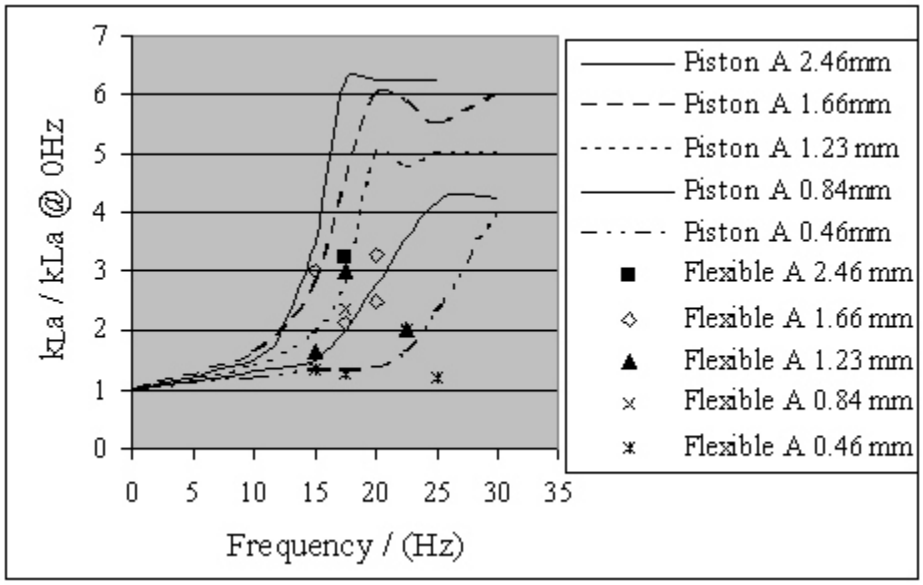

Figure 20b. k_La/k_La @ 0 Hz vs. Frequency
Solid piston vs. Flexible piston V = 30.4 ml/s

Applying Benjamin and Ursell Stability Theory to Resonate Bubble Breakage

It may be possible that observed resonance can be forecast by instability at the top interface. The inviscid theory of Benjamin and Ursell (1954) predicts the unstable wave motion of the free surface (air-water interface) of a water column subjected to vibrations at the base of the column.

We wish to assess if the instabilities predicted from the Matheau equations which arise in the Benjamin and Ursell (1954) analysis are also concomitant with resonance observed in our lab. Benjamin and Ursell (1954) show, under the assumptions of small vibrational amplitude, and negligible viscous and wall effects, the stability of the free surface is given by a series of Mathieu equations,

$$\frac{d^2 a_m}{dT^2} + \left(p_m - 2q_m (\cos 2T)\right) a_m = 0 \qquad (9)$$

where,

$$p_m = \left(\frac{4k_m \tanh(k_m h)}{\omega^2}\right)\left(g + \frac{k_m^2 \sigma}{\rho}\right) \qquad (10)$$

$$q_m = \frac{2k_m A \tanh(k_m h)}{\omega^2} \qquad (11)$$

a_m is the characteristic eigencoefficient; k_m is the characteristic eigenvalue; ω is the forcing frequency (radians/s) ; A is the amplitude (cm); h is the height of the water (cm), ρ is the water density = 1 g/cm^3; g is the acceleration due to gravity = 981cm/s^2; σ is the water surface tension = 72.5 dynes/cm; ρ is the density = 1 g/cc; and T is ½ ωt, where t is the time in s.

For a cylinder of radius R, k_m is defined as $k_{l,m}$ where $J'(k_{l,m} R) = 0$. Here m denotes the mth zero of the derivative of the lth order Bessel function.

In Figure 21 we have plotted the solid piston data from Table 9 using the results of Benjamin and Ursell (1954). Each frequency produces a constant p value and each fixed amplitude produces a constant q value. In Figure 21 we have used $(k_{l,m} R) = 11.706$, which is the 4th zero of the derivative of the first order (hence, l=1) Bessel function.

Notes
(1) k_m is calculated from R, and the number count on the series of eigenvalues (1, 2, 3 ....).
(2) l is sequential (0, 1, 2, 3, ...) And multiplies the equatorial angular position θ (i.e. cos lθ).

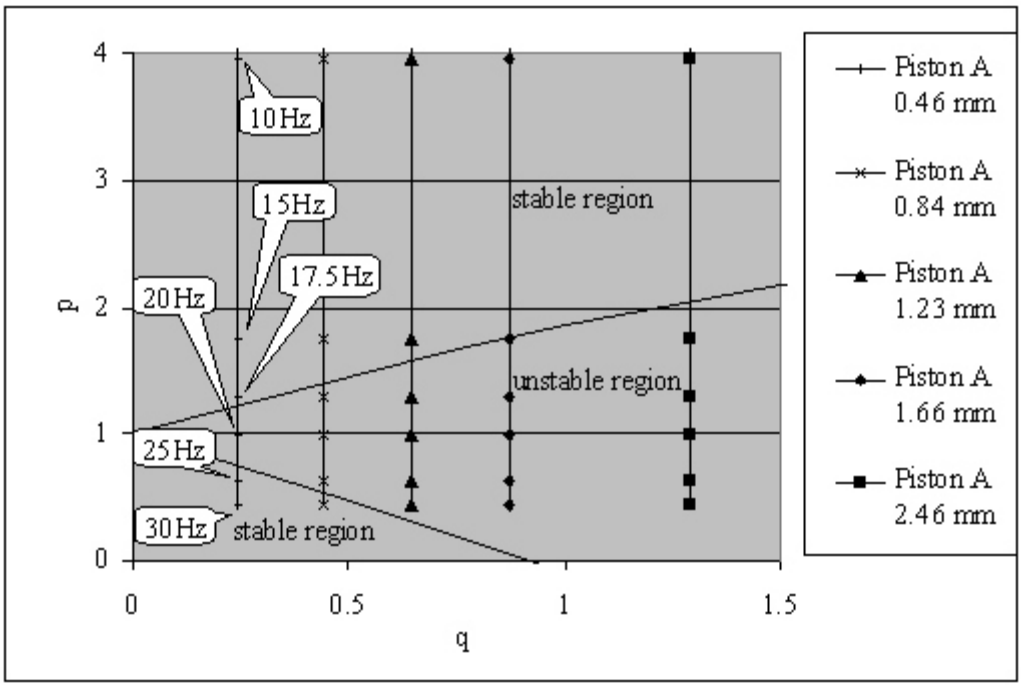

Figure 21. Column stability ($k_{1,4}R = 11.706$)

There appears to be close correlation based on the stability analysis of Benjamin and Ursell (1954) and the experimental data of Table 9. Free surface sloshing and/or foaming are strong indicators of instability. Data in Table 9 show excellent agreement with Figure 21, except for the smallest tested amplitude of 0.46 mm. For example at a constant amplitude of 1.23 mm, Figure 21 shows 0 - 15 hz to be stable but 17.5 - 30 hz to be unstable; this was experimentally observed (Table 9c). At the very small amplitude of 0.46mm, Figure 21 shows instability should occur at 20 Hz, however instability was experimentally observed at 30 Hz.

On could use the Benjamin and Ursell theory to predict operating regions with large mass transfer and voidage enhancements. However, an even easier approach may be to simply vary the frequency (starting at 0 Hz) at a chosen "cam setting" and wait for the surface to become unstable. There may be several frequency ranges which produce instability on the free surface, however the first range (15 - 30 Hz in our experiments) is expected to have the strongest resonant amplitude enhancement in the column. In short, observation of the top surface gives all the needed information to design for enhanced performance.

There is a word of caution when using the predictions of Benjamin and Ursell (1954). In Figure 21, it is taken to be true that the oscillation of the free surface is exactly ½ the forcing oscillation, as forecast by Benjamin and Ursell (1954). Also we have shown that action of the interface indicates conditions where bubble breakup will occur. Bubble breakup still occurs at the same experimental conditions if the interface is "quieted" by the addition of the Styrofoam disk as previously detailed.

Comparison of Induced Momentum and Resonant Bubble Breakage

As detailed previously, low flow rate induced momentum bubble breakage occurs as a result of suck-back and expulsion phenomena in the gas feeder tube. We have also shown bubble breakup at higher flowrates can be attributed to resonance effects in the fluid phase of the column. All available data for k_La are compiled in Table 10.

Table 10. Correlation of k_La with power term

GasFlow (ml/s)	U_{og} (SGV) (mm/s)	Flexible/Solid piston	k_La (s^{-1})	Frequency (Hz)	Amplitude (mm)	Omega (s^{-1})	$Rp^{0.25}$
30.4	4.89	F	0.004	0	0.74	0.00	1.00
30.4	4.89	F	0.0067	15	1.30	94.26	1.99
30.4	4.89	F	0.013	17.5	2.46	109.97	3.04
30.4	4.89	F	0.01	20	1.69	125.68	2.78
30.4	4.89	F	0.006	25	1.04	157.10	2.59
30.4	4.89	F	0.0042	0	0.30	0.00	1.00
30.4	4.89	F	0.0054	15	0.52	94.26	1.35
30.4	4.89	F	0.0095	17.5	0.84	109.97	1.81
30.4	4.89	F	0.0056	20	1.56	125.68	2.68
30.4	4.89	F	0.0048	25	0.39	157.10	1.64
20	3.21	F	0.0028	0	0.74	0.00	1.00
20	3.21	F	0.0045	15	1.30	94.26	2.20
20	3.21	F	0.0085	17.5	2.46	109.97	3.37
20	3.21	F	0.007	20	1.69	125.68	3.09
20	3.21	F	0.0043	25	1.04	157.10	2.87
20	3.21	F	0.0032	0	0.30	0.00	1.00
20	3.21	F	0.0039	15	0.52	94.26	1.46
20	3.21	F	0.0086	17.5	0.84	109.97	2.00
20	3.21	F	0.0042	20	1.56	125.68	2.97
20	3.21	F	0.0036	25	0.39	157.10	1.79
2	0.32	F	0.0006	0	0.74	0.00	1.00
2	0.32	F	0.001	15	1.30	94.26	3.88
2	0.32	F	0.00135	17.5	2.46	109.97	5.98
2	0.32	F	0.0011	20	1.69	125.68	5.48
2	0.32	F	0.001	25	1.04	157.10	5.09
2	0.32	F	0.0006	0	0.30	0.00	1.00
2	0.32	F	0.0007	15	0.52	94.26	2.47
2	0.32	F	0.00102	17.5	0.84	109.97	3.50

(table continued)

2	0.32	F	0.00095	20	1.56	125.68	5.27
2	0.32	F	0.00075	25	0.39	157.10	3.12
1.04	0.17	F	0.00054	0	0.74	0.00	1.00
1.04	0.17	F	0.00065	15	1.30	94.26	4.54
1.04	0.17	F	0.0008	17.5	2.46	109.97	7.01
1.04	0.17	F	0.00074	20	1.69	125.68	6.42
1.04	0.17	F	0.00074	25	1.04	157.10	5.96
1.04	0.17	F	0.00052	0	0.30	0.00	1.00
1.04	0.17	F	0.0006	15	0.52	94.26	2.88
1.04	0.17	F	0.00075	17.5	0.84	109.97	4.10
1.04	0.17	F	0.00065	20	1.56	125.68	6.17
1.04	0.17	F	0.00058	25	0.39	157.10	3.65
20	3.21	S	0.0032	0	1.23	0.00	1.00
20	3.21	S	0.0050	15	1.23	94.26	2.14
20	3.21	S	0.0064	17.5	1.23	109.97	2.40
20	3.21	S	0.0090	20	1.23	125.68	2.64
20	3.21	S	0.0143	25	1.23	157.10	3.11
30.4	4.89	S	0.0040	0	1.23	0.00	1.00
30.4	4.89	S	0.0078	15	1.23	94.26	1.94
30.4	4.89	S	0.0110	17.5	1.23	109.97	2.17
30.4	4.89	S	0.0200	20	1.23	125.68	2.38
30.4	4.89	S	0.0200	25	1.23	157.10	2.81
30.4	4.89	S	0.0040	0	0.46	0.00	1.00
30.4	4.89	S	0.0052	15	0.46	94.26	1.30
30.4	4.89	S	0.0052	17.5	0.46	109.97	1.41
30.4	4.89	S	0.0054	20	0.46	125.68	1.52
30.4	4.89	S	0.0092	25	0.46	157.10	1.76
30.4	4.89	S	0.0040	0	0.84	0.00	1.00
30.4	4.89	S	0.0052	15	0.84	94.26	1.64
30.4	4.89	S	0.0052	17.5	0.84	109.97	1.81
30.4	4.89	S	0.0054	20	0.84	125.68	1.99
30.4	4.89	S	0.0092	25	0.84	157.10	2.33
30.4	4.89	S	0.0040	0	1.66	0.00	1.00
30.4	4.89	S	0.0078	15	1.66	94.26	2.24
30.4	4.89	S	0.0110	17.5	1.66	109.97	2.50
30.4	4.89	S	0.0200	20	1.66	125.68	2.76
30.4	4.89	S	0.0200	25	1.66	157.10	3.26
30.4	4.89	S	0.0040	0	2.46	0.00	1.00

(Table continued)

30.4	4.89	S	0.0140	15	2.46	94.26	2.71
30.4	4.89	S	0.0250	17.5	2.46	109.97	3.04
30.4	4.89	S	0.0250	20	2.46	125.68	3.35
30.4	4.89	S	0.0250	25	2.46	157.10	3.96

One way to allow comparison of the data in Table 10 is to determine the power input to the system and then establish the expected relation between power and k_La. The advantage here is that all flow rate data using both the solid and flexible piston , can be plotted together. The power per unit mass, P_m, in a typical (non oscillating) BCR is simply taken as the superficial gas velocity, U_{og}

$$P_m = U_{og} \qquad (12)$$

The power per unit mass, P_m*, in an oscillating BCR is given by,

$$P_m^* = U_{og} + \frac{A^2\omega^3}{2} \qquad (13)$$

where the asterisk on P_m indicates the oscillating mode, A is the amplitude of liquid oscillation and ω is the frequency of oscillation. A simply ratio, R_p, of oscillating to non oscillating power is given by,

$$R_p = 1 + \frac{A^2\omega^3}{2gU_{og}} \qquad (14)$$

As shown by Rice et al.(1993), k_La is proportional to $(P_m)^{1/4}$. Therefore plots of k_La versus $(R_p)^{1/4}$ should be linear. In Figure 22a, data for both flexible and solid pistons at high and low flow rates are shown. The data clearly shows a well defined straight line at low flow rates. The apparent scatter in the high flow rate data can be explained. At high flow rates we have data at 0 Hz, 15 Hz, 17.5 Hz, 20 Hz, 25 Hz. We believe the data at 17.5 and 20 Hz show strong resonant enhancement. In Figure 22b, data are plotted for k_La versus $(R_p)^{1/4}$at the higher flowrates (20 and 30.4 ml/sec) leaving out the k_La values at 17.5 Hz and 20 Hz. The data in Figure 22b (without 17.5 and 20 Hz) fall on a straight line. In Figure 22c, the line determined from Figure 22b is again plotted and just the data at 17.5 and 20 Hz are added. The majority of this data falls well above the line which provides a strong indication of resonant bubble breakage and substantial energy savings at 17.5 and 20 Hz. Figures 22a and 22c provide strong evidence that two mechanisms are involved; low flow rates involve suck back and bubble breakup at the ejector tip and high flow rates involve column resonance effects at 17.5 and 20 Hz.

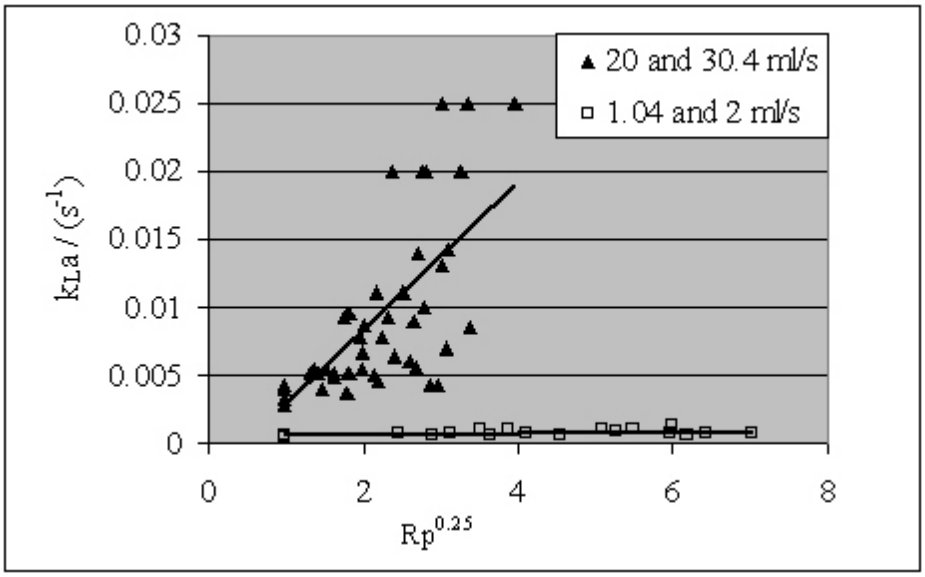

Figure 22a. k_La vs. $Rp^{0.25}$
(Flexible & solid piston at low and high gas flow rates)

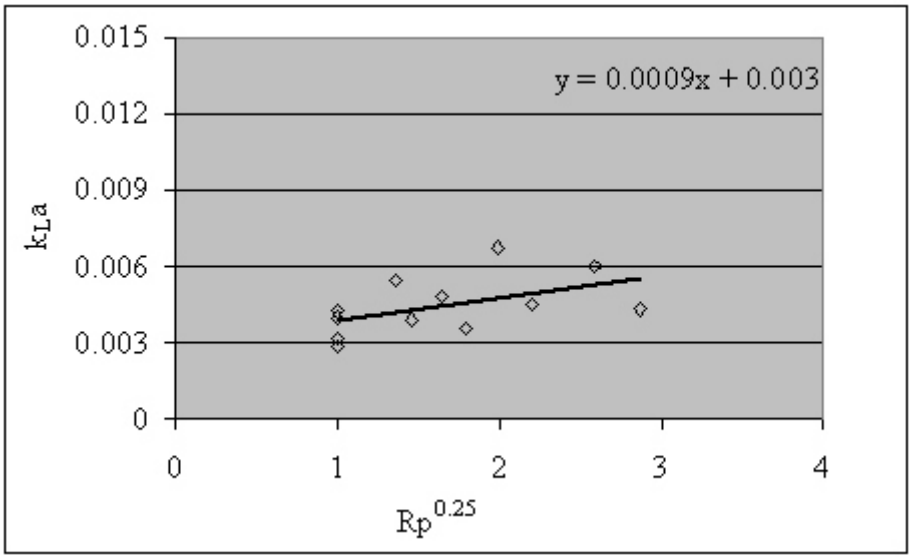

Figure 22b. k_La vs. $Rp^{0.25}$ at 20 and 30.4 ml/s
(Flexible piston leaving out 17.5 & 20 Hz)

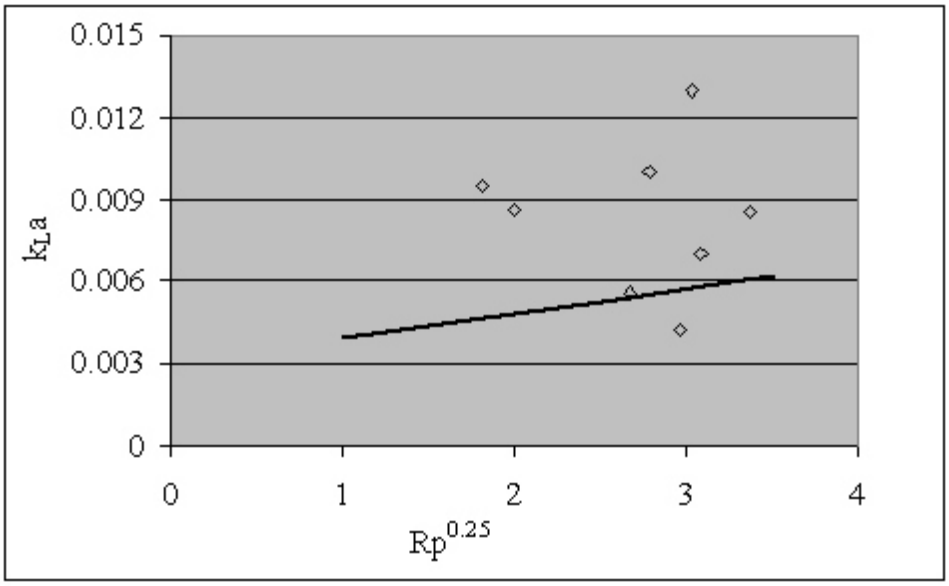

Figure 22c. k_La vs. $Rp^{0.25}$ at 20 and 30.4 ml/s
(Flexible piston only for 17.5 & 20 Hz)

Summary and Conclusion

Vibrating Bubble Column can generate large number of tiny bubbles under low forcing frequency (<30 Hz) and small forcing amplitude (<3 mm). Two different mechanisms are proposed to the phenomenal bubble breakup: induced shear slug breakage in the gas feeder tube for bubbly flow and resonant frequency bubble breakage in the column fluid phase for jet flow.

In the vibrating bubble column, mass transfer coefficient, k_La, is increased to 250 %~625 % of the no forcing value depending on flow regime and configuration of membrane and piston. Such a huge increase of k_La means that mass transfer is improved greatly.

Thanks to the substantial energy reductions and effective mass transfer improving, this technology can be applied to fermentation, phase transfer reaction system and waste water treatment process etc, particularly exciting for microscale reaction systems where methods of bubble generation and mixing are still at the exploratory level.

References

Baird, M.H.J. "Sonic resonance of bubble dispersions." *Chemical Engineering Science* **18**, p. 685-687 (1963).

Baird, M.H.J. "Resonant bubbles in a vertically vibrating liquid column." *The Canadian Journal of Chemical Engineering* **4** p. 52-55 (1963).

Bartsch,A. "Acceleration of mass transfer in gas liquid-reactions by sonic vibrations - fat hydrogenation as a test reaction." *Zeitschrift fur Naturforschung*, **50:(2-3)** p. 228-234 (1995).

Benjamin, T. B.; Ursell, F. "The stability of the plane free surface of a liquid in vertical periodic motion." *Proceedings of the Royal Society of London. Series A, Mathematical and Physical Sciences,* **225:1163** p. 505-515 September 22, 1954.

Burns, L.F. The effect of reduced surface tension an mass transfer and fluid dynamics in bubble column reactors (BCR), M.S. Thesis, Louisiana State Univesity (1995).

Connell, K.D. Mass transfer at an oscillating interface, B.S. Thesis, University of Queensland (1972).

Dodge, F.T. "Chapter 8 – Vertical excitation of propellant tanks" from "The dynamic behavior of liquids in moving containers" edited by Abramson, H.N. NASA-SP-106 (1966).

Ellenberger, J.; Krishan, R. "Improving mass transfer in gas-liquid dispersions by vibration excitement." *Chemical Engineering Science* **57**, p. 4809-4815 (2002).

Grinis, L.; Monin, Y. "Influence of vibrations on gas bubble formation in liquids." *Chemical Engineering Technology* **22:5**, p. 439-442 (1999).

Harbaum, K.L.; Houghton, G. "Effects of sonic vibrations on the rate of absorption of gases from bubble beds." *Chemical Engineering Science* **13**, p. 90-92 (1960).

Harbaum, K.L.; Houghton, G. "Effects of sonic vibrations on the rate of absorption of carbon dioxide in gas bubble-beds." *J. Appl. Chem.* **12**, p. 234-240 (1962).

Jameson, G. J; Davidson, J.F. "The motion of a bubble in a vertically oscillating liquid: theory for an inviscid liquid, and experimental results." *Chemical Engineering Science* **21**, p. 29-34 (1966).

Jameson, G. J. "The motion of a bubble in a vertically oscillating viscous liquid." *Chemical Engineering Science* **21**, p. 35-48 (1966).

Krishna, R.; Ellenberger, J.; Urseanu, M.I.; Keil, F.J. "Utilization of bubble resonance phenomena to improve gas - liquid contact." *Naturwissenschaften* **87**, p. 455-459 (2000).

Krishna, R.; Ellenberger, J. "Improving gas-liquid mass transfer in bubble columns by applying low-frequency vibrations." *Chemical Engineering Technology* **25:2**, p. 159-162 (2002a).

Krishna, J; Ellenberger, J. "Improving gas-liquid contacting in bubble columns by vibration excitement." *International Journal of Multiphase Flow* **28**, p. 1223-1234 (2002b).

Krishna, R.; Ellenberger, J. "Influence of low-frequency vibrations on bubble and drop sizes formed at a single orifice." *Chemical Engineering and Processing* **42**, p. 15-21 (2003).

Krischa,J; Kocamustafaogullari, G. "Breakup criteria for fluid particles." *International Journal of Multiphase Flow* **15(4)** p.573-588 (1989).

Kuesegen, R.; Fieg, F.; Bartsch, A.. "Method and device for introducing sound waves into reactors." United States Patent No: 6,318,888 B1. Nov. 20, 2001.

Lauterborn, W. "Numerical investigation of nonlinear oscillations of gas bubbles in liquids." *The Journal of the Acoustical Society of America* **59(2)**, p. 283-293 (1976).

Leighton, T.G.; Walton, A.J. "An experimental study of the sound emitted from gas bubbles in a liquid" *Eur. J. Phys.* **8**, p.98-104 (1987).

Leighton, T.G.; Wilkinson,M.; Walton, A.J.; Field, J.E. "Studies of non-linear bubble oscillations in a simulated acoustic filed" *Eur. J. Phys.* **11**, p.352-358 (1990).

Leighton, T.G.; Cox, B.T.; Phelps, A.D. "The Rayleigh-like collapse of a conical bubble" *The Journal of the Acoustical Society of America* **107(1)**, p. 130-142 (2000).

Letzel, H.M.; Schouten, J.C.; Krishna, R.; van den Bleek, C.M. "Gas holdup and mass transfer in bubble column reactors operated at elevated pressure." *Chemical Engineering Science* **54**, p. 2237-2246 (1999).

Minnaert, M. "On musical air-bubbles and the sounds of running water" *Phil. Mag.* **16**, p. 235-248 (1933).

Rallison, J.M. "The deformation of small and viscous drops and bubbles in shear flows." *Ann. Rev. Fluid Mech.* **16**, p. 45-66 (1984).

Rice, R.G.; Do, D.D. Applied Mathematics and Modeling for Chemical Engineers. John Wiley & Sons, Inc., 1995.

Rodriguez, P.; van Gundy, M.; Rice, R.G..; Knopf, F.C. “Mechanical sinusoidal forcing.” in preparation *Rev. Sci. Inst.* (2003).

Smith, F.D. “On the destructive mechanical effects fo the gas-bubbles liberated by the passage of intense sound through a liquid.”*Phil. Mag.* **19**, p. 1147-1151 (1935).

Strasberg, M. “The pulsation frequency of nonspherical gas bubbles in liquids. *The Journal of the Acoustical Society of America,* **25(3)**, p. 536-537 (1953).

Strasberg, M. “Gas bubbles as a source of sound in liquids” *The Journal of the Acoustical Society of America* **28(1)**, p. 20-26 (1956).

Wallis, G.B. One-dimensional two-phase flow. McGraw-Hill Book Company, 1969.

Wong, H.W.; Baird, M.H.I. “Fluidisation in a Pulsed Gas Flow.” *The Chemical Engineering Journal* **2**, p. 104-113 (1971).

Vita

Jia Ma (male), born on December 14, 1974, is from People's Republic of China. He got a bachelor of engineering degree in chemical engineering from Tianjin University in July 1995. Then he worked as an assistant engineer in Beijing Yanshan Petrochemical Corporation for two years. From September 1997 to July 2000, he studied in graduate school of Beijing University of Chemical Technology and obtained Master of Engineering degree in chemical engineering. In August 2000, he came to Department of Chemical Engineering in Louisiana State University. The degree of master of science in chemical engineering is expected on December 2003.